Adaptive mutability of colorectal cancers in response to targeted therapies

Adaptive mutability of colorectal cancers in response to targeted therapies

Mariangela Russo[1,2,*], Giovanni Crisafulli[1,2], Alberto Sogari[1,2], Nicole M. Reilly[3], Sabrina Arena[1,2], Simona Lamba[1], Alice Bartolini[1], Vito Amodio[1,2], Alessandro Magrì[1,2], Luca Novara[1], Ivana Sarotto[1], Zachary D. Nagel[4], Cortt G. Piett[4], Alessio Amatu[5,6], Andrea Sartore-Bianchi[5,6], Salvatore Siena[5,6], Andrea Bertotti[1,2], Livio Trusolino[1,2], Mattia Corigliano[7,8], Marco Gherardi[7,8], Marco Cosentino Lagomarsino[7,8], Federica Di Nicolantonio[1,2], Alberto Bardelli[1,2,*]

[1]Candiolo Cancer Institute, FPO – IRCCS, Str. Prov.le 142, km. 3,95, Candiolo (TO) 10060, Italy; [2]Department of Oncology, University of Torino, Str.Prov.le 142, km. 3,95, 10060 Candiolo (TO); [3]Fondazione Piemontese per la Ricerca sul Cancro ONLUS, Candiolo (TO), Italy; [4]Department of Environmental Health, JBL Center for Radiation Sciences, Harvard T.H. Chan School of Public Health, Boston, MA, USA; [5]Niguarda Cancer Center, Grande Ospedale Metropolitano Niguarda, 20162 Milan, Italy; [6]Department of Oncology and Hemato-Oncology, Università degli Studi di Milano, 20133 Milan, Italy; [7]IFOM-FIRC Institute of Molecular Oncology, Via Adamello 16, 20139 Milan, Italy; [8]Department of Physics, Università degli Studi di Milano, and I.N.F.N. 20133 Milan, Italy.

*Corresponding author. Email: alberto.bardelli@unito.it (A.B.); mariangela.russo@unito.it (M.R.)

Abstract

The emergence of drug resistance limits the efficacy of targeted therapies in human tumors. The prevalent view is that resistance is a fait accompli: when treatment is initiated, cancers already contain drug-resistant mutant cells. Bacteria exposed to antibiotics transiently increase their mutation rates (adaptive mutability), thus improving the likelihood of survival. We investigated whether human colorectal cancer (CRC) cells likewise exploit adaptive mutability to evade therapeutic pressure. We found that epidermal growth factor receptor (EGFR)/BRAF inhibition down-regulates mismatch repair (MMR) and homologous recombination (HR) DNA repair genes, and concomitantly up-regulates error-prone polymerases in drug-tolerant (persister) cells. MMR proteins were also down-regulated in patient-derived xenografts and tumor specimens during therapy. EGFR/BRAF inhibition induced DNA damage, increased mutability and triggered microsatellite instability. Thus, like unicellular organisms, tumor cells evade therapeutic pressures by enhancing mutability.

Over 75 years ago, Luria and Delbrück demonstrated that bacterial resistance to phage viruses was due to random mutations that spontaneously occurred in the absence of selection (*1*). Resistance to targeted therapies in human tumors is also widely thought to be due to mutations that exist prior to treatment (*2*). The conventional view is that relapses occur because drug-resistant mutant subclones are present in any detectable metastatic lesion prior to initiation of therapy. According to this view, resistance is a 'fait accompli', and the time to recurrence is merely the interval required for pre-existing drug resistant (mutant) cells to repopulate the lesion (*3*).

Here we explore the hypothesis that resistance to targeted therapies can also be fostered by a transient increase in genomic instability during treatment, leading to de novo mutagenesis. A similar process has been shown to increase the emergence of microbial strains resistant to antibiotics (*4, 5*). In a stable microenvironment, the mutation rate of microorganisms is usually low, which precludes the accumulation of deleterious mutations. However, several mechanisms of stress-induced genetic instability and increased mutability, known as stress-induced mutagenesis (SIM), have been described in bacteria and yeast (*6-12*).

Bacterial persister cells can survive lethal stress conditions imposed by antibiotics through a reduction in growth rate. A subsequent reduction in the efficiency of DNA mismatch repair (MMR) (*4, 9, 13*), and a shift to error-prone DNA polymerases increases the rate at which adaptive mutations occur in the surviving population (*4, 9, 14, 15*). Selection then allows the growth of mutant subpopulations capable of replicating under stressful conditions. Once the stressed population has adapted to the new conditions, the hypermutator status is counter-selected to avoid accumulation of deleterious mutations and to prevent the continuous increase of mutational load (*9, 16-20*). Together, these processes boost genetic diversity, foster adaptability to new microenvironments and contribute to the development of resistance (*9, 12, 18, 19*).

In the setting of cancer, the emergence of a drug tolerant persister population is often observed when oncogene-dependent tumor cells are challenged with targeted agents (*21*). Persister cancer cells survive exposure to targeted therapies through poorly understood mechanisms (*21*), and represent a reservoir from which genetically divergent, drug-resistant derivatives eventually emerge (*22, 23*). Recent work showed that drug-resistant mutant cancer cells can originate not only from rare, pre-existing mutant clones, but also from drug-tolerant sub-populations (*24*). The probability that the latter resistance mechanism occurs would be greatly increased if the genetic diversity of tumor cells was enhanced during treatment. Accordingly, we hypothesized that during the persister state tumor cells, like unicellular organisms, alter DNA repair and replication mechanisms to enhance adaptive mutability.

Targeted therapy-induced down-modulation of MMR and HR proficiency of CRC cells.

To test our hypothesis, we studied the response of microsatellite stable (MSS) human colorectal cancer (CRC) cell lines to the anti-EGFR (epidermal growth factor receptor) antibody cetuximab, which is approved, together with panitumumab, for treatment of patients with metastatic CRC whose tumors lack *RAS* and *BRAF* mutations (*25*); or with BRAF inhibitor dabrafenib as combinatorial treatment, which has shown promising activity in patients with CRC harboring *BRAF* mutations (*26*). We selected human CRC cell lines that are *RAS* and *BRAF* wild-type and sensitive to EGFR blockade (DiFi cells, fig. S1A), or that carry the oncogenic *BRAF* p.V600E mutation and are sensitive to concomitant EGFR and BRAF inhibition (WiDr cells, fig. S1A). Treatment with targeted agents led to G1 cell cycle arrest (fig. S1B). However, a small number of drug-tolerant persister cells survived several weeks after treatment initiation (fig. S1, C and D). Indeed, when drug pressure was removed, these cells rapidly resumed growth and again showed sensitivity to targeted therapy, thus demonstrating that persisters are only transiently and reversibly resistant to the treatment (fig. S1, E and F). In contrast, prolonged treatment led to the generation of permanently resistant cells, which did not re-acquire sensitivity after removal of drug pressure (fig. S1, E and F).

We next assessed whether CRC cells modulate the expression of DNA repair genes upon drug treatment. Transcriptional profiles revealed decreased expression of the MMR genes *MLH1*, *MSH2*, *MSH6*, as well as homologous recombination (HR) effectors, such as *BRCA2* and *RAD51* (**Fig. 1A**, fig. S1, G and H). Expression of *EXO1*, a gene coding for an exonuclease that participates in mismatch and double-strand break (DSB) repair, was also affected (**Fig. 1A**, fig. S1, G and H). A time-dependent down-regulation of MMR and HR proteins was also observed (**Fig. 1B,** fig. S2, A and B). Comparable results were obtained in another cetuximab-sensitive human CRC cell line, NCIH508 (fig. S3, A to C), and in *BRAF*-mutant HT29 cells that were derived from the same patient from whom the WiDr cell line originated (fig. S3, D and E). Furthermore, we confirmed that down-regulation or loss of DNA repair components is maintained in persister cells (fig. S4, A to D). Therapy-induced modulation of DNA repair genes expression was transient and expression levels returned to normal upon removal of treatment (fig. S5A). Cancer cells that had previously developed permanent resistance to targeted agents did not modulate expression of DNA repair genes in response to drugs (fig. S5, B and C).

To ascertain whether targeted therapies affect DNA repair competence in CRC cells, we used fluorescence-based multiplex host cell reactivation (FM-HCR) assays (*27*). CRC cells were transfected with a G:G mismatch-containing plasmid to determine the impact of drug treatment on MMR capacity. A MMR deficient (MMRd) human CRC cell line (LIM1215) was used as a positive control for MMR loss. We found that in CRC cells treated with targeted agents, MMR proficiency (MMRp) was reduced to levels comparable to those observed in LIM1215 (**Fig. 1C,** fig. S6A).

We next evaluated cellular HR capability by using the two-step, plasmid-based, pDRGFP/pCBASce-I assay (*28*). Upon stable expression of the pDRGFP plasmid, we measured the generation of a green fluorescent signal upon DSBs induced by Sce-I expression. By this assay, both DiFi and WiDr cells showed a marked reduction in HR proficiency upon treatment with targeted therapies (**Fig.1D**, fig. S6B).

MMR proteins are down-regulated in samples of CRC residual disease after targeted treatment.

To determine whether the cell-based findings extend to patient-derived tumor samples, we exploited our CRC biobank of molecularly and therapeutically annotated patient-derived xenograft (PDX) models (*29, 30*). We selected six MSS PDX models with wild-type *KRAS*, *NRAS* and *BRAF* in which EGFR inhibition by cetuximab led to tumor regression to a variable extent, paralleling the clinical scenario (**Fig. 2A**). Immunohistochemistry analysis unveiled areas with down-regulation of MLH1 and/or MSH2 in all neoplastic samples obtained when tumors were at the point of maximum response to cetuximab, but still contained residual persisters (**Fig. 2B and C,** fig. S7, A to D), as compared with placebo-treated controls.

We next investigated whether down-regulation of DNA repair proteins also occurs in clinical specimens from two CRC patients who achieved an objective partial response upon treatment with FOLFOX plus panitumumab. In both instances, tumor specimens were longitudinally collected at diagnosis and at maximal therapeutic response, when a limited number of tumor cells persist despite treatment. MLH1 and MSH2 were down-regulated in tumor samples obtained at response compared to pre-treatment specimens, confirming the clinical relevance of our findings (**Fig. 2D**).

Induction of DNA damage and error-prone DNA polymerases in CRC cells treated with targeted therapies.

In addition to reduced DNA repair ability, we found that targeted therapies triggered a switch from high-fidelity to low-fidelity DNA polymerases. DNA polymerases usually involved in accurate DNA replication, such as POLδ and POLε were down-regulated; whereas DNA polymerases characterized by poor accuracy, low processivity and absence of proofreading capacity (i.e., error-prone polymerases) were induced (**Fig. 1A,** fig. S4A). These included Polι, Polκ, and Rev1 (which belong to Y family polymerases, orthologous to the bacterial stress-induced polymerases Pol IV and Pol V), as well as Polλ and Polμ, (*31*) (**Fig. 1 A and B**; figs S1, G and H; S2B; S3, B to C and E; S4, A and D). Error-prone polymerases replace canonical high-fidelity polymerases that stall when encountering a DNA lesion, and facilitate DNA replication across DNA damage sites in a manner that introduces errors into the genome (*15, 16, 20*); this may lead to bases mispairings, incorporation of aberrant DNA primer ends, and increased mutagenesis rate (*32, 33*).

We therefore investigated whether treatment with targeted therapies leads to genomic damage in cancer cells, and if error-prone mediated repair of DNA damage was favored when CRC cells encountered the hostile environment imposed by targeted therapies. Indeed, quantification of phosphorylation of H2AX at Ser 139 (γH2AX), a common marker of DNA damage (*34*), revealed a dose- and time-dependent increase in the number of foci-positive nuclei upon drug treatment (**Fig. 3 A and B,** fig. S8, A and B), while no further increase was observed in permanently resistant cells upon drug treatment (fig. S8, C and D). In addition, we observed a dose- and time-dependent increase in the number of 53BP1-positive nuclei upon EGFR and BRAF blockade (fig. S9, A and B). In direct opposition to BRCA1, 53BP1 promotes non-homologous end joining (NHEJ)-mediated DSB repair while preventing HR through restriction of end resection (*35*). These data suggest that targeted therapies trigger a switch from high-fidelity to error-prone mediated repair of DNA damage, thereby potentially increasing the occurrence of mutations conferring drug resistance.

We next explored the possible causes of the DNA damage observed upon targeted therapies administration. While several chemotherapeutic agents directly generate DNA damage, drugs interfering with oncogenic signaling (such as EGFR or BRAF inhibitors) are not directly genotoxic. Intriguingly, however, it has been shown that certain targeted therapies, such as ABL and BRAF inhibitors, increase the levels of reactive oxygen species (ROS) in cancer cells (*36, 37*), potentially contributing to DNA damage during treatment. ROS levels significantly increased when CRC cells were exposed to EGFR and BRAF inhibitors (**Fig. 3C**). In contrast, ROS levels were not increased in permanently drug-resistant (adapted) cells upon drug treatment (fig. S9C).

The drug-induced increase in ROS levels was abrogated when targeted therapies were administered in the presence of the antioxidant N-acetyl-L-cysteine (NAC) (**Fig. 3C**). NAC administration partially reduced the number of γH2AX foci-positive nuclei upon EGFR and BRAF blockade (fig. S10, A and B). However, co-treatment with NAC did not prevent or rescue down-regulation of DNA repair genes (fig. S10C). Notably, addition of NAC delayed onset of relapse to targeted therapies when administered together with MAPK pathway inhibitors (fig. S10, D and E)(*38, 39*).

Interfering with oncogenic dependencies initiates stress response in CRCs.

To elucidate the mechanistic basis of therapy-induced mutagenesis in cancer cells, we tested whether the adaptive mutability that we observed in response to targeted therapies was simply a secondary response to G1 cell cycle arrest or DNA damage, or whether it represented an active stress-response. We found that thymidine-mediated cell cycle stress (fig. S11, A to C) or direct DNA damage with the alkylating agent oxaliplatin (fig. S11, D to F) rather promoted up-regulation of the MMR and HR repair systems (fig. S11C and F); while G1 cell cycle arrest by nutrient starvation did not lead to modulation of DNA repair gene expression (fig. S11, G to I). In bacterial cells, both the DNA damage-activated SOS response and the general stress response appear to be required to induce adaptive mutagenesis (*14*). We therefore examined the modulation of the kinase

mammalian target of rapamycin (mTOR), which is a master regulator of mammalian cellular stress response (*40*). Indeed, the mTOR effectors pS6K–p70K were down-regulated with kinetics comparable to that of MMR and HR modulation, upon EGFR and BRAF pharmacological blockade (**Fig. 3D**). However, silencing of mTOR did not affect expression of DNA repair proteins or γH2AX (**Fig. 3E**). It is therefore plausible that down-regulation of mTOR contributes to stress-induced mutagenesis of cancer cells but is not sufficient to activate this phenotype.

The exquisite sensitivity of DiFi and WiDr cells to EGFR and BRAF blockade reflects cell-specific oncogenic alterations. The *EGFR* locus is amplified in DiFi cells (*2*); the WiDr cells carry the *BRAF* p.V600E oncogenic mutation, but they also become dependent on feedback activation of EGFR when treated with BRAF inhibitors (*41*). We therefore assessed whether interfering with the oncogenic dependency of cancer cells could directly initiate the drug-induced stress phenotype. Indeed, siRNA-mediated knock-down of *EGFR* or *KRAS* in DiFi cells, and *BRAF* (+/- *EGFR*) in WiDr cells led to reduced expression of DNA repair proteins, triggered DNA damage and mTOR down-modulation (**Fig. 3E**), and increased ROS levels (fig. S12). These results exclude the possibility that drug-induced down-modulation of DNA repair pathways could be due to a nonspecific (off-target) effect of the anti-EGFR antibody cetuximab or the BRAF inhibitor dabrafenib.

Targeted therapies induce adaptive mutability in CRC cells.

Next, we tested whether the stress response induced by targeted therapies translated into increased mutagenesis in CRC cells. We used a reporter assay in which a dinucleotide CA-repeat microsatellite drives the NanoLuc enzyme coding sequence out-of-frame (**Fig. 4A**). Random mutations that introduce frameshifts in this region, in absence of a functional MMR, would restore the NanoLuc open reading frame leading to bioluminescence. Analogous approaches have previously been used to measure MMR defects in cancer cells (*42-44*). To validate the assay, we first introduced the CA-NanoLuc vector into a MMRd human CRC cell line (HCT116) and three MMRp human CRC cell lines (DiFi, WiDr, NCIH508). The NanoLuc signal was significantly higher in MMRd cells after 48 hours of standard growth conditions (**Fig. 4B**). This difference was further increased when HCT116 were kept in culture for several days, while the signal in the MMRp lines remained low (**Fig. 4B**), indicating that the CA-NanoLuc assay effectively detects MMR deficiency in cancer cells.
We next used the CA-NanoLuc system to measure the impact of ectopic inactivation of MMR in CRC cells. To this end, we used CRISPR-CAS9 to inactivate the *MLH1* gene in HT29 human CRC cell line. After the isolation of two independent *MLH1* knock-out (KO) clones (fig. S13, A and B), they were transduced with the CA-NanoLuc vector. *MLH1* KO clones exhibited higher levels of NanoLuc signal as expected, confirming that the assay can detect inactivation of DNA MMR (**Fig. 4C**). Next, drug-dependent (transient) MMR down-regulation was evaluated. EGFR and BRAF inhibition led to time-dependent increases of bioluminescence (**Fig. 4D**), paralleling the down-regulation of DNA repair effectors and up-regulation of low-fidelity polymerases. We further found that

permanently resistant derivatives no longer exhibited adaptive mutability in response to targeted therapies (fig. S14).

Genomic alterations in CRC cells upon treatment with targeted therapies.

To determine whether molecular evidence of adaptive mutability was present in the genome of CRC cells treated with EGFR and BRAF inhibitors, we analyzed whole-exome sequencing (WES) data from DiFi and WiDr parental, persister, and drug-resistant derivative cells. The overall mutational burden (number of mutations/megabase) of persisters, and drug resistant cell population was only marginally affected (fig. S15, A and B). As a control, we assessed whether MMR permanent inactivation, induced by *MLH1* KO, affected the mutational burden of HT29 CRC cells, and found that it was only marginally affected (fig. S16A).
We therefore changed approach. Since treatment with targeted therapies led to a transient MMR deficient phenotype, we reasoned that MMR status could be more easily detected by examining microsatellite regions, where DNA replication slippage errors occur frequently and are ineffectively repaired in the absence of MMR. Indeed, WES analysis unveiled alterations in microsatellite regions of HT29 in which the *MLH1* gene was genetically knocked-out (fig. S16, B and C). Importantly, we also detected increased genetic instability in the microsatellite regions of CRC cells made resistant to targeted agents (**Fig. 5, A and B**), as shown by a shift in the length of microsatellite regions, highlighting the impact of targeted therapies on DNA repair process and mutagenicity. To detect the occurrence of microsatellite alterations in non-clonal cell populations, we utilized a high depth capture panel that detects hotspot somatic variants as well as shifts in length of microsatellite regions. Indeed, such high sensitivity analysis unveiled a significant shift in the length of microsatellite regions in both persister and drug-resistant cells (**Fig. 5 C,** fig. S17).

We next assessed the impact of targeted therapies on the genomic landscape of PDXs. To do this, we studied a PDX (CRC0078) (**Fig. 2A,** fig. S7D) that was continuously treated with cetuximab until it developed resistance (fig. S18). WES analysis of the cetuximab-resistant tumor tissue revealed alterations in microsatellite genomic regions which were not present in the PDX tumor collected from the corresponding untreated mouse (**Fig. 5, D and E**). Overall, these results indicate that CRC cells and a CRC PDX exposed to targeted therapies experience loss of replication fidelity in regions of nucleotide repeats.

Discussion

The development of resistance has emerged as a major limitation of targeted therapies directed against oncoproteins, such as EGFR, BRAF and ABL (*25*).

In this study, we tested the hypothesis that cancer cells treated with targeted therapies activate stress-induced mutagenic mechanisms. We found that persister (drug-tolerant) cancer cells that survive EGFR and/or BRAF inhibition exhibit DNA damage, down-regulate mismatch and homologous recombination

repair proteins, switch from high-fidelity to error-prone DNA repair, and transiently increase their mutagenic ability.

Stress-induced mutagenesis is a characteristic trait of unicellular organisms to transiently accelerate genetic diversity, in a fraction of the population, when encountering a hostile environment. (*16*). Indeed, we found that therapy-induced modulation of DNA repair in cancer cells is also transitory and reverts back once a mutational landscape able to restore the ability to grow in the presence of the drug is achieved. We postulate that in cells of multicellular organisms, stress-induced mutagenesis is not operational. However, in cancer cells that have lost tissue-imposed homeostasis, and in many ways operate like unicellular organisms, this ancestral program is still available and is unleashed by oncoprotein-targeted drugs. A similar process has also been observed in cancer cells undergoing hypoxia-driven stress (*7, 45, 46*).

The analysis of mutational signatures has emerged as a valuable tool to document the mutational processes operative in cells (*47*). In future studies, it will be interesting to establish whether specific mutational signatures emerge under targeted therapies. Resolving such processes, which we postulate occur transiently in small cell subpopulations, is likely to require extensive genomic comparisons of multiple clones and independent datapoints.

These results may have clinical implications. The knowledge that cancer cells under therapeutic stress down-regulate key effectors of the DNA repair machinery, such as MMR and HR, exposes a vulnerability that could be clinically exploited. For example, it will be important to assess whether down-regulation of HR proteins confers sensitivity to poly-ADP-ribose polymerases (PARP) inhibitors as observed in HR deficient cancers (*48-50*). Moreover, pharmacological or genetic interference could be deployed to curb the cellular mechanisms that initiate drug-driven adaptive mutagenesis with the goal of reducing the generation of new variants during treatment. This strategy could potentially increase and prolong the clinical efficacy of targeted therapies.

References and Notes

1. S. E. Luria, M. Delbrück, Mutations of Bacteria from Virus Sensitivity to Virus Resistance. *Genetics* **28**, 491-511 (1943).
2. S. Misale *et al.*, Emergence of KRAS mutations and acquired resistance to anti-EGFR therapy in colorectal cancer. *Nature* **486**, 532-536 (2012).
3. L. A. Diaz *et al.*, The molecular evolution of acquired resistance to targeted EGFR blockade in colorectal cancers. *Nature* **486**, 537-540 (2012).
4. A. Gutierrez *et al.*, β-Lactam antibiotics promote bacterial mutagenesis via an RpoS-mediated reduction in replication fidelity. *Nat Commun* **4**, 1610 (2013).
5. H. Long *et al.*, Antibiotic treatment enhances the genome-wide mutation rate of target cells. *Proc Natl Acad Sci U S A* **113**, E2498-2505 (2016).

6. I. Bjedov *et al.*, Stress-induced mutagenesis in bacteria. *Science* **300**, 1404-1409 (2003).
7. D. M. Fitzgerald, P. J. Hastings, S. M. Rosenberg, Stress-Induced Mutagenesis: Implications in Cancer and Drug Resistance. *Annu Rev Cancer Biol* **1**, 119-140 (2017).
8. P. L. Foster, Stress-induced mutagenesis in bacteria. *Crit Rev Biochem Mol Biol* **42**, 373-397 (2007).
9. R. S. Galhardo, P. J. Hastings, S. M. Rosenberg, Mutation as a stress response and the regulation of evolvability. *Crit Rev Biochem Mol Biol* **42**, 399-435 (2007).
10. E. Shor, C. A. Fox, J. R. Broach, The yeast environmental stress response regulates mutagenesis induced by proteotoxic stress. *PLoS Genet* **9**, e1003680 (2013).
11. E. Heidenreich, Adaptive mutation in Saccharomyces cerevisiae. *Crit Rev Biochem Mol Biol* **42**, 285-311 (2007).
12. D. M. Fitzgerald, S. M. Rosenberg, What is mutation? A chapter in the series: How microbes "jeopardize" the modern synthesis. *PLoS Genet* **15**, e1007995 (2019).
13. G. P. Rodriguez *et al.*, Mismatch repair-dependent mutagenesis in nondividing cells. *Proc Natl Acad Sci U S A* **109**, 6153-6158 (2012).
14. R. G. Ponder, N. C. Fonville, S. M. Rosenberg, A switch from high-fidelity to error-prone DNA double-strand break repair underlies stress-induced mutation. *Mol Cell* **19**, 791-804 (2005).
15. G. J. McKenzie, S. M. Rosenberg, Adaptive mutations, mutator DNA polymerases and genetic change strategies of pathogens. *Curr Opin Microbiol* **4**, 586-594 (2001).
16. P. L. Foster, Adaptive mutation: implications for evolution. *Bioessays* **22**, 1067-1074 (2000).
17. F. Taddei *et al.*, Role of mutator alleles in adaptive evolution. *Nature* **387**, 700-702 (1997).
18. J. Torkelson *et al.*, Genome-wide hypermutation in a subpopulation of stationary-phase cells underlies recombination-dependent adaptive mutation. *EMBO J* **16**, 3303-3311 (1997).
19. W. A. Rosche, P. L. Foster, The role of transient hypermutators in adaptive mutation in Escherichia coli. *Proc Natl Acad Sci U S A* **96**, 6862-6867 (1999).
20. G. J. McKenzie, R. S. Harris, P. L. Lee, S. M. Rosenberg, The SOS response regulates adaptive mutation. *Proc Natl Acad Sci U S A* **97**, 6646-6651 (2000).
21. S. V. Sharma *et al.*, A chromatin-mediated reversible drug-tolerant state in cancer cell subpopulations. *Cell* **141**, 69-80 (2010).
22. G. R. Oxnard, The cellular origins of drug resistance in cancer. *Nat Med* **22**, 232-234 (2016).
23. M. Ramirez *et al.*, Diverse drug-resistance mechanisms can emerge from drug-tolerant cancer persister cells. *Nat Commun* **7**, 10690 (2016).
24. A. N. Hata *et al.*, Tumor cells can follow distinct evolutionary paths to become resistant to epidermal growth factor receptor inhibition. *Nat Med* **22**, 262-269 (2016).

25. S. Misale, F. Di Nicolantonio, A. Sartore-Bianchi, S. Siena, A. Bardelli, Resistance to anti-EGFR therapy in colorectal cancer: from heterogeneity to convergent evolution. *Cancer Discov* **4**, 1269-1280 (2014).
26. S. Kopetz *et al.*, Encorafenib, Binimetinib, and Cetuximab in. *N Engl J Med*, (2019).
27. Z. D. Nagel *et al.*, Multiplexed DNA repair assays for multiple lesions and multiple doses via transcription inhibition and transcriptional mutagenesis. *Proc Natl Acad Sci U S A* **111**, E1823-1832 (2014).
28. A. J. Pierce, R. D. Johnson, L. H. Thompson, M. Jasin, XRCC3 promotes homology-directed repair of DNA damage in mammalian cells. *Genes Dev* **13**, 2633-2638 (1999).
29. A. Bertotti *et al.*, The genomic landscape of response to EGFR blockade in colorectal cancer. *Nature* **526**, 263-267 (2015).
30. C. Isella *et al.*, Selective analysis of cancer-cell intrinsic transcriptional traits defines novel clinically relevant subtypes of colorectal cancer. *Nat Commun* **8**, 15107 (2017).
31. A. J. Rattray, J. N. Strathern, Error-prone DNA polymerases: when making a mistake is the only way to get ahead. *Annu Rev Genet* **37**, 31-66 (2003).
32. V. M. Krutiakov, [Eukaryotic error prone DNA polymerases: suggested roles in replication, repair and mutagenesis]. *Mol Biol (Mosk)* **40**, 3-11 (2006).
33. M. F. Goodman, Error-prone repair DNA polymerases in prokaryotes and eukaryotes. *Annu Rev Biochem* **71**, 17-50 (2002).
34. L. J. Mah, A. El-Osta, T. C. Karagiannis, gammaH2AX: a sensitive molecular marker of DNA damage and repair. *Leukemia* **24**, 679-686 (2010).
35. S. Panier, S. J. Boulton, Double-strand break repair: 53BP1 comes into focus. *Nat Rev Mol Cell Biol* **15**, 7-18 (2014).
36. G. Cesi, G. Walbrecq, A. Zimmer, S. Kreis, C. Haan, ROS production induced by BRAF inhibitor treatment rewires metabolic processes affecting cell growth of melanoma cells. *Mol Cancer* **16**, 102 (2017).
37. M. Koptyra *et al.*, BCR/ABL kinase induces self-mutagenesis via reactive oxygen species to encode imatinib resistance. *Blood* **108**, 319-327 (2006).
38. M. L. Sagristá, A. E. García, M. Africa De Madariaga, M. Mora, Antioxidant and pro-oxidant effect of the thiolic compounds N-acetyl-L-cysteine and glutathione against free radical-induced lipid peroxidation. *Free Radic Res* **36**, 329-340 (2002).
39. E. D. Chan, D. W. Riches, C. W. White, Redox paradox: effect of N-acetylcysteine and serum on oxidation reduction-sensitive mitogen-activated protein kinase signaling pathways. *Am J Respir Cell Mol Biol* **24**, 627-632 (2001).
40. R. A. Saxton, D. M. Sabatini, mTOR Signaling in Growth, Metabolism, and Disease. *Cell* **168**, 960-976 (2017).
41. A. Prahallad *et al.*, Unresponsiveness of colon cancer to BRAF(V600E) inhibition through feedback activation of EGFR. *Nature* **483**, 100-103 (2012).
42. J. Shen *et al.*, ARID1A deficiency promotes mutability and potentiates therapeutic antitumor immunity unleashed by immune checkpoint blockade. *Nat Med* **24**, 556-562 (2018).

43. N. Chatterjee, Y. Lin, B. A. Santillan, P. Yotnda, J. H. Wilson, Environmental stress induces trinucleotide repeat mutagenesis in human cells. *Proc Natl Acad Sci U S A* **112**, 3764-3769 (2015).
44. R. Parsons *et al.*, Hypermutability and mismatch repair deficiency in RER+ tumor cells. *Cell* **75**, 1227-1236 (1993).
45. V. T. Mihaylova *et al.*, Decreased expression of the DNA mismatch repair gene Mlh1 under hypoxic stress in mammalian cells. *Mol Cell Biol* **23**, 3265-3273 (2003).
46. R. S. Bindra, P. M. Glazer, Co-repression of mismatch repair gene expression by hypoxia in cancer cells: role of the Myc/Max network. *Cancer Lett* **252**, 93-103 (2007).
47. M. Petljak *et al.*, Characterizing Mutational Signatures in Human Cancer Cell Lines Reveals Episodic APOBEC Mutagenesis. *Cell* **176**, 1282-1294.e1220 (2019).
48. L. Li, H. Wang, E. S. Yang, C. L. Arteaga, F. Xia, Erlotinib attenuates homologous recombinational repair of chromosomal breaks in human breast cancer cells. *Cancer Res* **68**, 9141-9146 (2008).
49. S. Nowsheen *et al.*, Cetuximab augments cytotoxicity with poly (adp-ribose) polymerase inhibition in head and neck cancer. *PLoS One* **6**, e24148 (2011).
50. J. Mateo *et al.*, A decade of clinical development of PARP inhibitors in perspective. *Ann Oncol*, (2019).
51. M. Russo *et al.*, Reliance upon ancestral mutations is maintained in colorectal cancers that heterogeneously evolve during targeted therapies. *Nat Commun* **9**, 2287 (2018).
52. G. Germano *et al.*, Inactivation of DNA repair triggers neoantigen generation and impairs tumour growth. *Nature* **552**, 116-120 (2017).
53. K. Wang *et al.*, MapSplice: accurate mapping of RNA-seq reads for splice junction discovery. *Nucleic Acids Res* **38**, e178 (2010).
54. B. Li, C. N. Dewey, RSEM: accurate transcript quantification from RNA-Seq data with or without a reference genome. *BMC Bioinformatics* **12**, 323 (2011).
55. J. Harrow *et al.*, GENCODE: the reference human genome annotation for The ENCODE Project. *Genome Res* **22**, 1760-1774 (2012).
56. A. Gnirke *et al.*, Solution hybrid selection with ultra-long oligonucleotides for massively parallel targeted sequencing. *Nat Biotechnol* **27**, 182-189 (2009).
57. G. Siravegna *et al.*, Radiologic and Genomic Evolution of Individual Metastases during HER2 Blockade in Colorectal Cancer. *Cancer Cell* **34**, 148-162.e147 (2018).
58. G. Corti *et al.*, A Genomic Analysis Workflow for Colorectal Cancer Precision Oncology. *Clin Colorectal Cancer* **18**, 91-101.e103 (2019).
59. B. Niu *et al.*, MSIsensor: microsatellite instability detection using paired tumor-normal sequence data. *Bioinformatics* **30**, 1015-1016 (2014).
60. S. R. Kennedy *et al.*, Detecting ultralow-frequency mutations by Duplex Sequencing. *Nat Protoc* **9**, 2586-2606 (2014).
61. M. W. Schmitt *et al.*, Sequencing small genomic targets with high efficiency and extreme accuracy. *Nat Methods* **12**, 423-425 (2015).

Acknowledgments
We thank members of Molecular Oncology Laboratory at Candiolo Cancer Institute for critically reading the manuscript. We also thank A. Cassingena and F. Sassi for their help with experiments. We also thank Grahame Mckenzie for the NanoLuc plasmid design.
Funding: The research was supported by Fondazione AIRC under 5 per Mille 2018 - ID. 21091 program – P.I. Bardelli Alberto, G.L. Siena Salvatore, G.L. Bertotti Andrea, G.L Trusolino Livio, G.L. Di Nicolantonio Federica; AIRC 2010 Special Program Molecular Clinical Oncology 5 per mille, Project n. 9970 Extension program (A.B.); AIRC IG n. 16788 (A.B.); AIRC IG 2018 - ID. 21923 project - PI Bardelli Alberto (A.B.); H2020 grant agreement no. 635342-2 MoTriColor (A.B.); Ministero Salute, Ricerca Corrente 2019 RC2019 (A.B.); H2020 grant agreement no. 754923 COLOSSUS (L.T.). A.B. has received research funding from PhoreMost and NeoPhore.
Author contributions: M.R. and A.B. conceived the study. M.R., A.S., N.M.R., S.A., S.L., V.A., A.M. M.C., M.G. and M.C.L. conducted the experiments and analyzed data. G.C. performed NGS and bioinformatics analysis. Ali.B. performed NGS panel-based experiments. L.N. performed RNAseq bioinformatics analysis. N.Z. and C.P. provided plasmids harboring DNA damage. And.B. and L.T. analyzed and provided PDX material. I.S. performed and analyzed IHC data; A.A., A.S.B. and S.S. provided patient samples. F.D.N. analyzed data. M.R. and A.B. wrote the manuscript. A.B. supervised the study.
Competing interests: L.T. is a paid consultant for Eli Lilly, AstraZeneca, and Merck KGaA. ZDN is an inventor on a patent (U.S. 9,938,587) covering methods and kits for determining DNA repair capacity. A.B. is a member of the scientific advisory board of NeoPhore and a shareholder of NeoPhore and PhoreMost. The other authors declare no competing interests.
Data and materials availability: The FM-HCR reporter plasmids are available from ZDN under a Material Transfer Agreement. The pDRGFP and the pCBASce-I plasmids are available from AddGene under a Material Transfer Agreement. The NanoLuc expressing plasmid is available from PhoreMost Ltd (Cambridge, UK) under a Material Transfer Agreement. The HT29 Empty and *MLH1* knock-out cells are available from AB (UNITO) under a Material Transfer Agreement. RNA-seq data and DNA seq data are deposited in ENA (from EBI) - #PRJEB28674.

List of Supplementary Materials:

Materials and Methods

Figures S1-S18

Tables S1 to S2

References (*51-61*)

Figure Legends

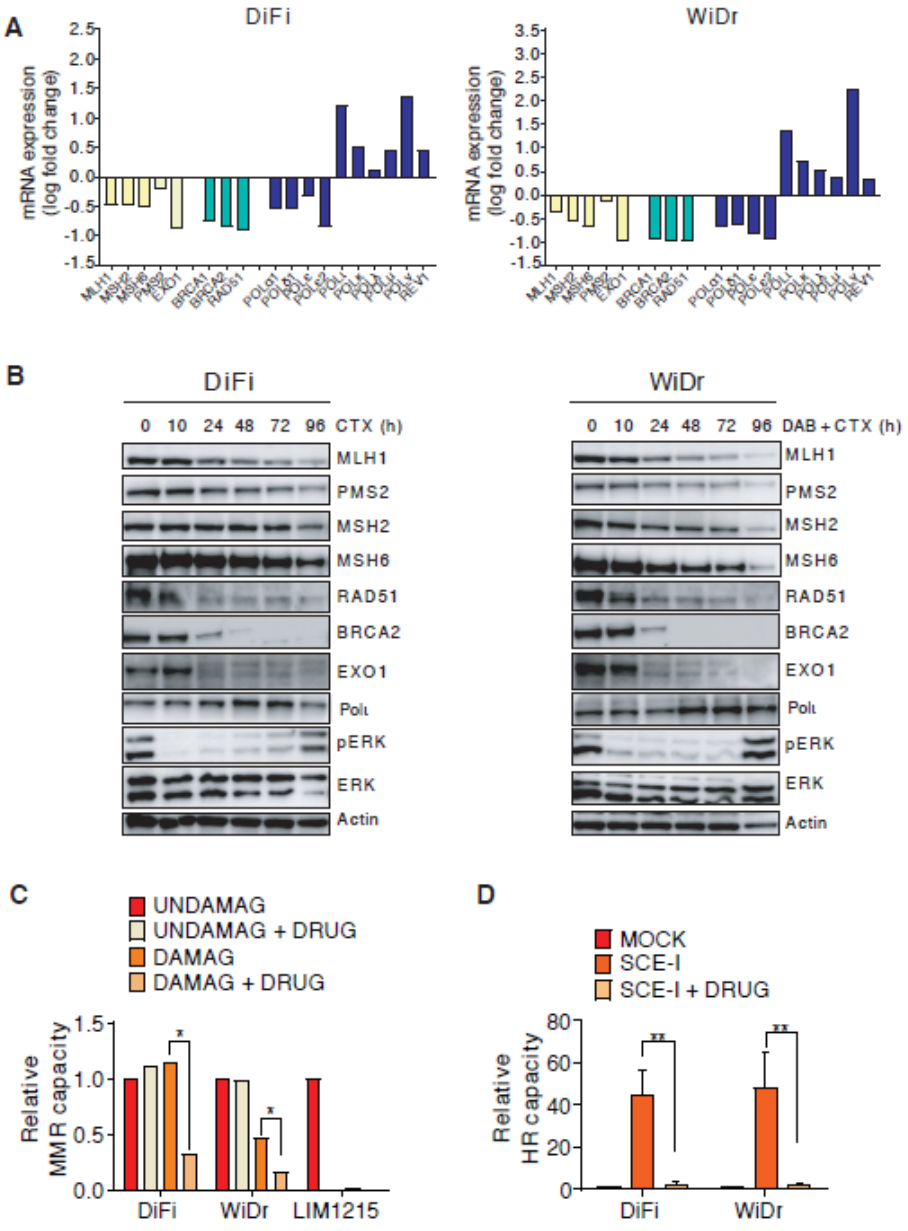

Fig. 1. CRC cells modulate DNA repair effectors in response to targeted agents. (A) CRC cells were treated with cetuximab alone (DiFi) or in combination with the BRAF inhibitor dabrafenib (WiDr) for 96h and RNAseq analysis was performed. Mismatch repair (MMR) (yellow), homologous recombination (HR) (green), and DNA polymerases (blue) genes are reported. Results represent means of two independent experiments. (B) CRC cells were treated and analyzed at indicated time points by Western blot. (C) CRC cells were transfected with G:C undamaged (UNDAMAG) plasmid or with G:G mismatch-damaged (DAMAG) plasmid. Where indicated (DRUG), cells were treated with targeted therapies for fifty-sixty hours and analyzed by flow cytometry. A mock transfection was used as control. Quantification of MMR capacity of each cell line

relative to control is reported in the bar graph. MMR deficient CRC cells LIM1215 were used as a positive control for MMR loss. Results represent means of two independent experiments. *p< 0.05 (Student's t test). (D) pDRGFP-stably expressing CRC cells were transfected with the pCBASce-I plasmid and then either left in the absence of drug or treated with targeted therapies for fifty-sixty hours and analyzed by flow cytometry. A mock transfection was used as control. Quantification of HR capacity of each cell line relative to mock is reported in the bar graph. Results represent means ± SD (n=3). ** p< 0.01 (Student's t test).

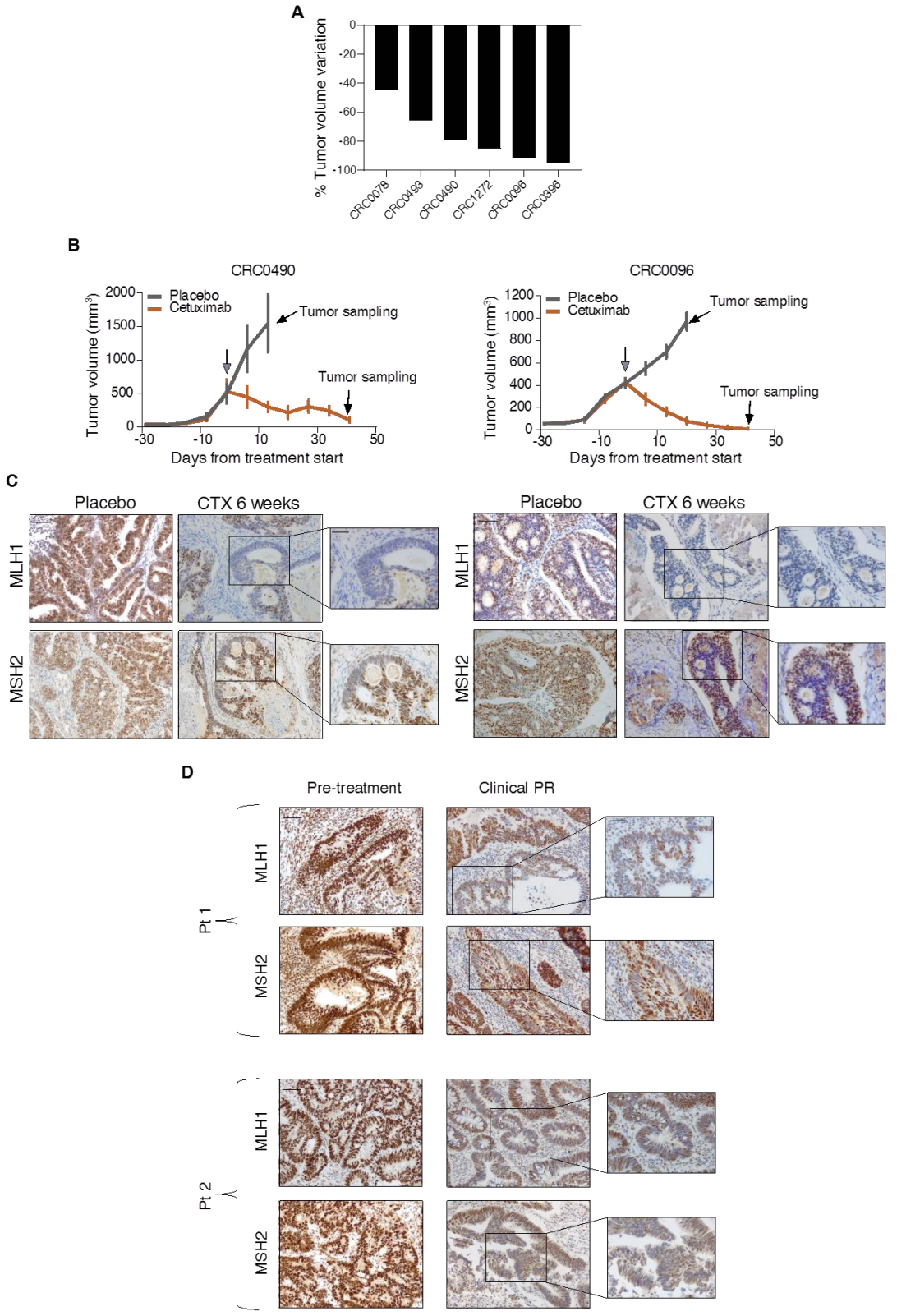

Fig. 2. MMR down-regulation in CRC PDXs and patients treated with targeted therapies. (A) Extent of tumor regression in PDX models after treatment with cetuximab (20 mg/kg twice weekly) for six weeks. Each bar is the average of tumor volumes from 6 mice. (B) Growth curve kinetics in two out of six PDXs. Mean tumor volumes ± SEM (*n*=6). Gray arrows, treatment initiation. (C) Immunohistochemical staining with anti-MLH1 and anti-MSH2 antibodies of histologic tumor sections derived from indicated PDXs treated with cetuximab

for six weeks. Tumor section derived from placebo arm was used as control. Scale bar 0.1mm. Magnifications ×40 (scale bar 0.05mm). (D) Immunohistochemical staining with anti-MLH1 and anti-MSH2 antibodies of tumor sections derived from two CRC patients treated with FOLFOX+anti-EGFR monoclonal antibody panitumumab. Tumor sections were derived from the primary lesion at diagnosis (pre-treatment), and at the time of partial response (PR) when the lesions shrank. Scale bar 0.1mm. Magnifications ×40 (scale bar 0.05mm).

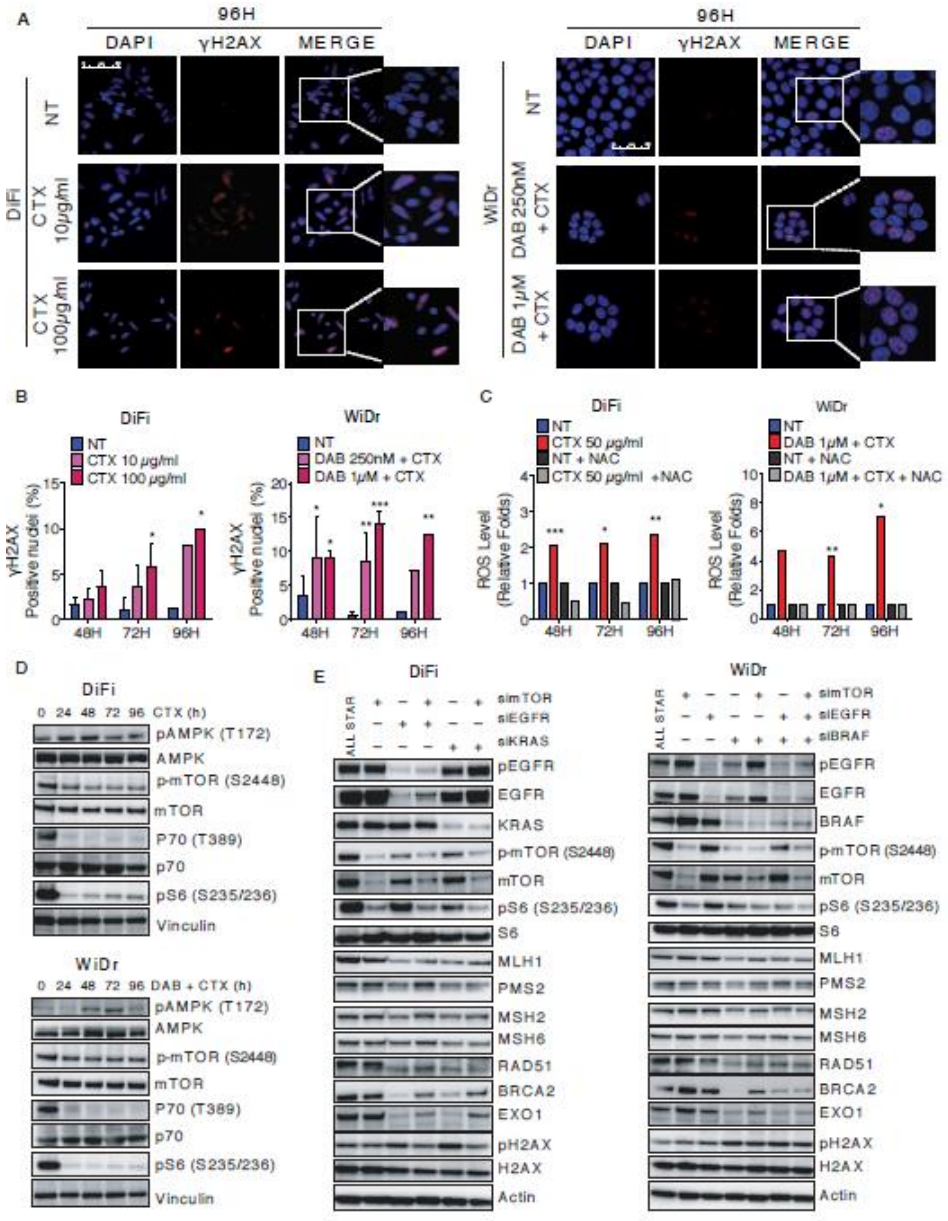

Fig. 3. Targeted therapies trigger stress response, increase ROS levels and induce DNA damage in CRC cells. (A) CRC cells were treated as reported and fixed and stained with anti-γH2AX antibody at indicated time points. Vehicle treated cells (NT) were used as control. Nuclei are stained with DAPI (blue) and anti-γH2AX antibody (red). Scale bar: 50μm. Representative images for each condition are shown. (B) Quantification of nuclear γH2AX foci in DiFi (left panel)

and WiDr (right panel) cells. Results represent means ± SD (n=3 for 48 and 72H; n=2 for 96H). *p< 0.05; **p< 0.01; ***p< 0.001 (Two Way ANOVA). (C) CRC cells were treated as indicated and ROS levels were measured. NAC was used as a control to rescue ROS production. Results represent means of two independent experiments. *p< 0.05; **p< 0.01; ***p< 0.001 (Student's t test). (D) CRC cells were treated with targeted therapies and analyzed by Western blot at indicated time points. (E) WT DiFi (left panel) and *BRAF*-mutated WiDr (right panel) cells were transfected with indicated siRNA or combinations of them for 72 hours and analyzed by Western blot. All star, non-targeting siRNA.

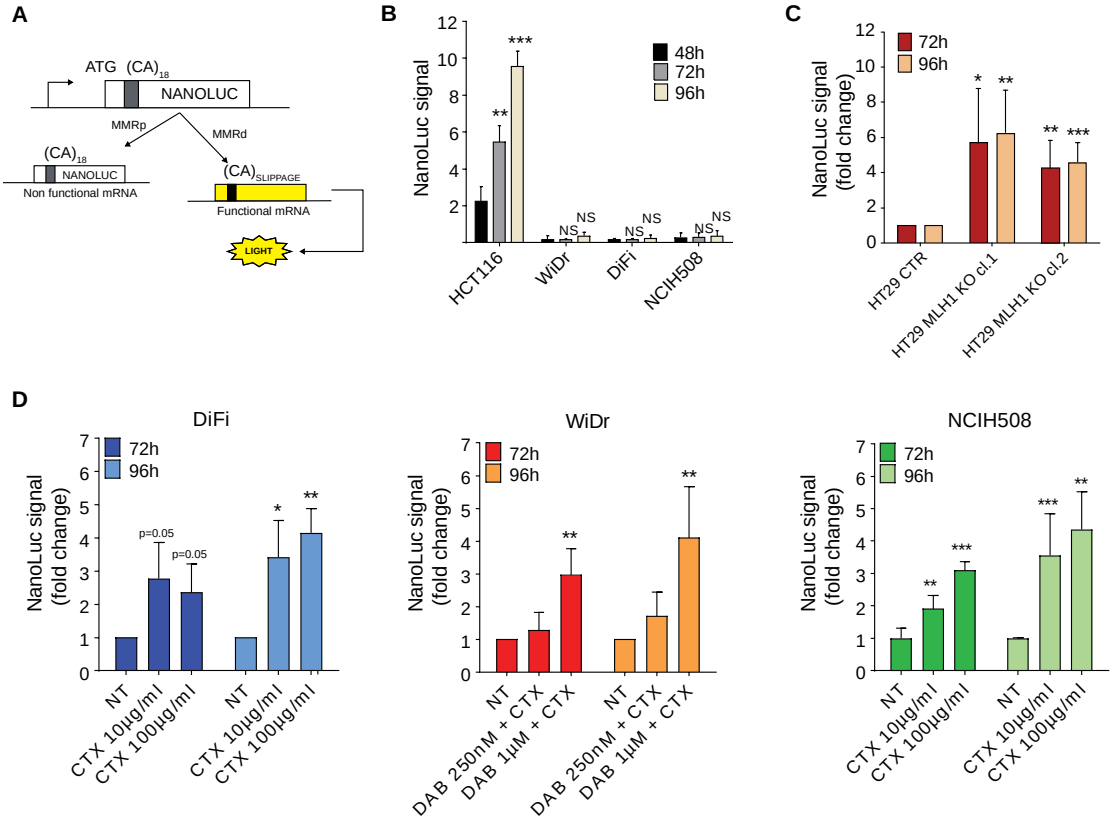

Fig. 4. Treatment with targeted therapies promotes mutagenesis in CRC cells. (A) Schematic representation of the CA-NanoLuc reporter assay. MMRp, mismatch repair proficient; MMRd, mismatch repair deficient. (B) MMRd HCT116 and MMRp DiFi, WiDr and NCIH508 CRC cells were transduced with the NanoLuc lentivirus. At indicated time points NanoLuc signal was evaluated and normalized to cell viability. Results represent means ± SD (n=3). **p< 0.01; ***p < 0.001 (Student's t test). Ns, not statistically significant differences. (C) NanoLuc signal in HT29 *MLH1* knock-out (KO) clones (cl. 1 and cl. 2). NanoLuc signal was evaluated after 72 and 96 hours of growth in standard conditions and normalized to cell viability. NanoLuc signal from *MLH1* KO clones was then compared to signal detected in *MLH1* WT cells (CTR). Results represent means ± SD (n=4). *p < 0.05; **p < 0.01; ***p < 0.001 (Student's t test). (D) DiFi, WiDr, and

NCIH508 CRC cells were treated as indicated. NanoLuc signal was normalized to cell viability. NanoLuc signal from treated cells was then compared to signal detected in untreated (NT) cells. Results represent means ± SD (n=3). *$p < 0.05$; **$p < 0.01$; ***$p < 0.001$ (Student's t test).

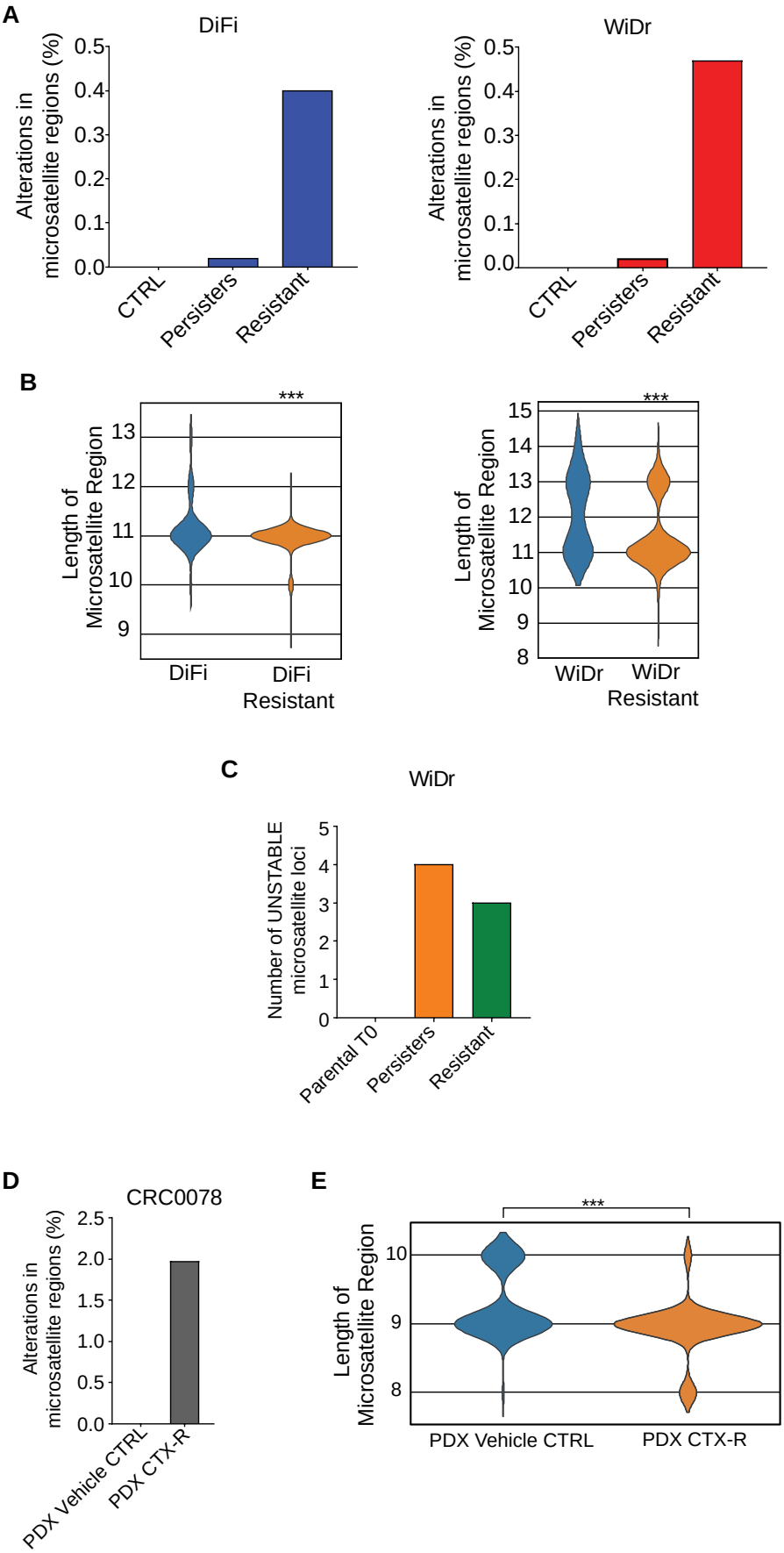

Fig. 5. Adaptive mutability leads to genetic instability in CRC cells in response to therapy-induced stress. (A) Percentage of unstable microsatellite

regions in DiFi and WiDr persister and resistant cells compared to their parental counterpart (CTRL). (B) Length distribution of one representative microsatellite region for drug-resistant DiFi and WiDr cell lines. ***p< 0.001 ($\chi 2$ test). (C) Number of unstable microsatellite sites detected by NGS-based high depth capture panel in WiDr cells (parental); treated with cetuximab + dabrafenib for 14 days (persisters) and at resistance. (D) DNA was collected from one vehicle-treated and from one cetuximab-resistant PDX. Percentage of unstable microsatellite regions of the tumor collected from the cetuximab-resistant mouse (PDX CTX-R) as compared to the vehicle-treated (CTRL) mouse is reported. (E) Length distribution of one representative microsatellite region. ***p < 0.001 ($\chi 2$ test).

Science
AAAS

Supplementary Materials for

Adaptive mutability of colorectal cancers in response to targeted therapies

Mariangela Russo[1,2,*], Giovanni Crisafulli[1,2], Alberto Sogari[1,2], Nicole M. Reilly[3], Sabrina Arena[1,2], Simona Lamba[1], Alice Bartolini[1], Vito Amodio[1,2], Alessandro Magrì[1,2], Luca Novara[1], Ivana Sarotto[1], Zachary D. Nagel[4], Cortt G. Piett[4], Alessio Amatu[5,6], Andrea Sartore-Bianchi[5,6], Salvatore Siena[5,6], Andrea Bertotti[1,2], Livio Trusolino[1,2], Mattia Corigliano[7,8], Marco Gherardi[7,8], Marco Cosentino Lagomarsino[7,8], Federica Di Nicolantonio[1,2] and Alberto Bardelli[1,2,*]

*Corresponding author. Email: alberto.bardelli@unito.it (A.B.); mariangela.russo@unito.it (M.R.)

This PDF file includes:

Materials and Methods

Cell culture and generation of resistant CRC cells

Cells were routinely supplemented with FBS 10%, 2mM L-glutamine, antibiotics (100U/mL penicillin and 100 mg/mL streptomycin) and grown in a 37°C and 5% CO_2 air incubator. Cells were routinely screened for absence of Mycoplasma contamination using the Venor® GeM Classic kit (Minerva biolabs). The identity of each cell line was checked no more than three months before performing experiments by PowerPlex® 16 HS System (Promega), through Short Tandem Repeats (STR) tests at 16 different loci (D5S818, D13S317, D7S820, D16S539, D21S11, vWA, TH01, TPOX, CSF1PO, D18S51, D3S1358, D8S1179, FGA, Penta D, Penta E, and amelogenin). Amplicons from multiplex PCRs were separated by capillary electrophoresis (3730 DNA Analyzer, Applied Biosystems) and analyzed using GeneMapper v.3.7 software (Life Technologies). Persister cells were generated through continuous treatment for 2 weeks with 100μg/ml of anti-EGFR monoclonal antibody cetuximab (DiFi) or with 50μg/ml of cetuximab in combination with 1μM BRAF inhibitor dabrafenib (WiDr). Resistant cell lines employed in this study have been previously described (*2, 51*).

Cetuximab was kindly provided by MERCK Group.

Drug proliferation assays

CRC cells were seeded at different densities (2-5x10^3 cells/well) in medium containing 10% FBS in 96-well plastic culture plates at day 0. The following day, serial dilutions of the indicated drugs were added to the cells in serum-free medium (ratio 1:1), while DMSO-only treated cells were included as controls. Plates were incubated at 37°C in 5% CO_2 for the indicated time. Cell viability was assessed by measuring ATP content through Cell Titer-Glo® Luminescent Cell Viability assay (Promega).

Time-To-Progression (TTP) assay

For the TTP long-term assay, 5 million cells were plated in their respective growth media, as previously described (*51*), and treated from the following day with 100µg/ml cetuximab alone (DiFi), 50µg/ml cetuximab + 1µM dabrafenib (WiDr), 10mM NAC or a combination of the drugs as indicated. Cells were counted once a week. Counts reported as "0" represent time points in which cells were too few to be counted and only medium and drug refreshments were done.

Q-RT-PCR

Prior to analysis, cells were grown in their specific media supplemented with 10% FBS and treated as follow: 100µg/ml of cetuximab (CTX) for DiFi and NCIH508; 50µg/ml cetuximab (CTX) + 1µM dabrafenib (DAB) for WiDr and HT29. Total RNA was extracted from CRC cells using Maxwell® RSC miRNA Tissue Kit (Promega), according to the manufacturer's protocol. The quantification and quality analysis of RNA was performed by Thermo Scientific Nanodrop 1000 and Bioanalyzer 2100 (Agilent Technologies). DNA was transcribed using iScript RT Super Mix (BioRad) following the manufacturer's instructions. Q-RT-PCR was performed in triplicate on an ABI PRISM 7900HT thermal cycler (Life Technologies) with SYBR green (Promega) dye (MLH1, MSH2, MSH6, Polι) or TaqMan (Thermofisher) probes (BRCA1, BRCA2, EXO1, and Polκ). SDHA and GAPDH expression levels were used for normalization. The sequences of the primers (IDT) used for gene expression analyses were: MLH1 FW 5'-CAGAGCTTGGAGGGGGATA-3'; MLH1 REV 5'- TTTCGGGAATCATCTTCCAC -3'; MSH2 FW 5'- AACCCAAATCCATCGTAGGT -3'; MSH2 REV 5'- AACCCAAATCCATCGTAGGT -3'; MSH6 FW 5'- GGGGCAAGTCTACGCTTATG -3'; MSH6 REV 5'- CACACTTCAGCAGGGACGTA -3'; POLι FW 5'- ACAAACCGGGATTTCCTACC-3'; POLι REV 5'-TCACACTTCCTTTCCCTTGAA-3'; SDHA FW 5'- TGGGAACAAGAGGGCATCTG-3';SDHA REV 5'- CCACCACTGCATCAAATTCATG-3'. Taqman probe (ThermoFisher scientific) used are as follows: BRCA1 (Hs01556190_m1); BRCA2(Hs00609073_m1); EXO1 (Hs00243513_m1); Pol κ (Hs00211965_m1), and GAPDH (Hs99999905_m1).

Western blotting analysis

Prior to biochemical analysis, cells were grown in their specific media supplemented with 10% FBS and treated as follow: 100µg/ml of cetuximab (CTX) for DiFi and NCIH508; 50µg/ml cetuximab (CTX) + 1µM dabrafenib (DAB) for WiDr and HT29. Following treatment, total cellular proteins were extracted by solubilizing the cells in boiling SDS buffer (50 mM Tris-HCl [pH 7.5], 150 mM

NaCl, and 1% SDS). Samples were boiled for 5 minutes at 95°C and sonicated for 10 seconds. Extracts were clarified by centrifugation and normalized with the BCA Protein Assay Reagent kit (Thermo). Western blot detection was performed with enhanced chemiluminescence system (GE Healthcare) and peroxidase conjugated secondary antibodies (Amersham). The following primary antibodies were used for western blotting: anti-MLH1 (abcam; 1:5000); anti-MSH2 (abcam; 1:5000); anti-MSH6 (abcam; 1:5000); anti-PMS2 (Cell Marque Corporation, USA; 1:10); anti EXO1 (abcam; 1:1000); anti-RAD51 (GeneTex; 1:500); anti BRCA2 (Cell Signaling; 1:1000); anti-Polι (abcam; 1:1000); anti–phospho-p44/42 ERK (Thr202/Tyr204) (Cell Signaling; 1:1000); anti-ERK (Cell Signaling; 1:1000); anti-p-EGFR (Tyr1068) (Cell Signalling; 1:1000); anti-EGFR (EnzoLifeSciences; 1:1,00); anti-BRAF (Santa Cruz; 1:500); anti-KRAS (Sigma Aldrich; 1:1000); anti-actin (Santa Cruz; 1:3000); anti-Vinculin (Millipore; 1:3000); anti-p-mTOR (Ser2448) (Cell Signaling; 1:1000); anti-mTOR (Cell Signaling; 1:1000); anti-p-p70S6K (Thr389) (Cell Signaling; 1:1000); anti-p70S6K Cell Signaling; 1:1000); anti-p-S6 (Ser235/236) (Cell Signaling; 1:1000); anti-p-AMPK (Thr172) (Cell Signaling; 1:1000); anti-AMPK (Cell Signaling; 1:1000); anti-pH2AX (Ser139) (Cell Signaling; 1:1000); anti-H2AX (Cell Signaling; 1:1000).

Cell cycle analysis

CRC cells were seeded at different densities (2-3x10^5 cells/well) in complete medium in 6-well plastic culture plates at day 0. The following day, the indicated treatments were added. Plates were incubated at 37°C in 5% CO_2 for the indicated time. Following treatment, cells were stained with Propidium Iodide (Sigma Aldrich) following manufacturer's instructions and analyzed by flow cytometry.

Immunohistochemistry

Patient tumor samples were obtained under the approval of the local Ethical committee of the Niguarda Cancer Center (MI) and of the Italian Ministry of Health. Tumor sections were formalin-fixed, paraffin-embedded, and processed according to standard procedures using Envision Flex+, Mouse, High pH (DAKO) and PT link (DAKO). Sections were analyzed with the following antibodies: anti-MLH1 (BD transduction Laboratories; 1:40); anti-MSH2 (Calbiochem; 1:50).

Immunofluorescence

CRC cells, grown on glass coverslip, were fixed in 4% paraformaldehyde for 20 min at RT and permeabilized with 0.1% Triton-X100 in PBS for 2 min on ice. Then, cells were treated at RT with 1% BSA in PBS for 30 min and incubated for 2h at room temperature (RT) with the following primary antibodies diluted in PBS containing 1% of BSA and 1% of donkey serum: anti-MLH1 (BD Pharmigen) (1:200); anti-Polι (1:200) (GeneTex). After washing, cells were fluorescently labeled, according to the primary antibody used, with an Alexa Fluor® 555 donkey anti-mouse antibody or Alexa Fluor® 488 donkey anti-rabbit antibody (Molecular Probes, Eugene, USA) diluted 1:400 in PBS containing 1% BSA and donkey serum for 1h. Nuclei were stained with DAPI. F-actin was stained with Alexa Fluor® 647 Phalloidin (50 μg/ml). Slides were then mounted using the fluorescence mounting medium (Dako, Glostrup, DK) and analyzed using a confocal laser scanning microscope (TCS SPE II; Leica, Wetzlar, D). For

immunofluorescence detection of γ-H2AX and 53BP1 foci, cells were stained with the anti-phospho-Histone H2AX (Ser139) rabbit monoclonal antibody (Bethyl Laboratories) (1:600), anti-53BP1 rabbit polyclonal antibody (Cell Signaling) (1:100) and Alexa555 goat anti-rabbit IgG secondary (Thermo Fisher) (1:400). A Leica DMI6000B fluorescence microscope (Leica Microsystems, Wetzlar, Germany) under a 40X dry objective was used to detect γ-H2AX and 53BP1 foci. Images were captured at 10 individual z-planes and were merged using the "Z Project" function in ImageJ. Individual nuclei were scored for foci positivity as identified based upon signal intensity above general background staining levels and presence within the nucleus as assessed by DAPI staining. Cells containing ≥ 5 distinct foci were defined as foci-positive, and the percentage of positive nuclei was calculated as [(number of γ-H2AX foci positive nuclei) / (number of nuclei scored)]* 100. A minimum of 500 nuclei per sample were scored and the data shown were collected from two biological replicates. Statistical significance of the experimental data was determined using Two-Way ANOVA as indicated in the figure legend in GraphPad (Prism7). Where indicated, CRC cells were treated as follow: 10 or 100μg/ml of cetuximab (CTX) for DiFi; 50μg/ml cetuximab (CTX) + 250nM or 1μM dabrafenib (DAB) for WiDr at indicated time points.

CRC cell transduction

The NanoLuc expressing plasmid was provided by PhoreMost Ltd (Cambridge, UK). The sequence of the NanoLuc enzyme (NanoLuc® Promega) is cloned downstream of a stretch of 18 CA-dinucleotide repeats (microsatellite region). In this condition, the luciferase cDNA is out-of-frame and does not encode a functional enzyme. The random introduction of indels in the CA18 sequence restores the NanoLuc open reading frame and leads to the expression of the NanoLuc measurable by luminescence. Lentiviral particles were generated by co-transfection of HEK293T cells with the viral vector and packaging plasmids pVSVg (AddGene #8454) and psPAX2 (AddGene #12260). CRC cell lines were seeded at 25 × 10^4 cells/well in 6-well plastic culture plates. The following day, cells were infected with lentivirus at approximately 80% confluence in the presence of 8μg/mL polybrene (Millipore). Seventy-two hours after infection, puromycin (Sigma Aldrich) or blasticidin (Gibco) were used to select stably infected cells.

NanoLuc assay

CRC cells were seeded at 2-3x10^3 cells/well in 96-well plastic cell culture plates at day 0. The following day, cells were treated with targeted therapies as follow: 10 or 100μg/ml of cetuximab (CTX) for DiFi and NCIH508; 50μg/ml cetuximab (CTX) + 250nM or 1μM dabrafenib (DAB) for WiDr at indicated time points. At the end of treatment, NanoLuc expression was measured using NanoGlo® Luciferase Assay System (Promega) according to manufacturer's instruction. Luminescence was measured by TECAN Spark® Plate reader. The NanoLuc signal was normalized to the viability measured through Cell Titer-Glo®Luminescent Cell Viability assay (Promega).

MMR assay

The MMR assay was performed as previously described (*27*). Cells were seeded at 25 × 10^4 cells/well in 6-well plastic culture plates. The following day, cells were transfected with a mixture containing 700ng of pmax-vector; 150ng of pmax-BFP and 150ng pmax-mOrange (G:C undamaged control) or with pmax-G:G-mismatch containing-mOrange (damaged MMR) using Lipofectamine 3000 following manufacturer's instruction. The MMR reporter is designed to express a non-fluorescent orange protein unless the site-specific G:G mismatch is repaired in a manner that restores the wild-type sequence in the transcribed strand (*27*). Immediately after transfection, cells were treated as follow: 100µg/ml cetuximab (CTX) for DiFi or 50µg/ml cetuximab (CTX) + 1µM dabrafenib (DAB) for WiDr. Fifty to sixty hours after transfection cells were harvested and analyzed by flow cytometry. The pmax-BFP was used as internal control for transfection efficiency to normalize the mOrange signal. The relative MMR capacity was determined by dividing the percentage of mOrange positive cells in damaged MMR by the percentage of mOrange positive cells in undamaged control.

Generation of pDRGFP expressing cells

The CRC cells WiDr and DiFi were seeded at 25 × 10^4 cells/well in 6-well plastic culture plates. The following day, cells were transfected with pDRGFP plasmid (AddGene) using Lipofectamine 3000 following manufacturer's instruction. pDRGFP plasmid is composed of two differentially mutated GFP (green fluorescent protein) genes oriented as direct repeats and separated by a drug selection marker (*28*). One of the GFP genes is mutated to contain the recognition site for the Sce-I endonuclease and, as a result, will undergo a DSB when Sce-I is ectopically expressed (*28*). A homologous recombination event between the two GFP genes results in the expression of intact GFP protein. Seventy-two hours after infection, puromycin (Sigma Aldrich) was used to select stably infected cells.

HR assay

The pDRGFP-expressing cells were seeded at 25 × 10^4 cells/well in 6-well plastic culture plates. The following day, cells were transfected with the Sce-I -expressing plasmid (pCBASce-I; AddGene) (*28*) using Lipofectamine 3000 following manufacturer's instruction. Immediately after transfection, cells were treated with 100µg/ml cetuximab (DiFi) or with 50µg/ml cetuximab + 1µM dabrafenib (WiDr). Fifty to sixty hours after transfection, cells were harvested and analyzed by flow cytometry. The relative HR capacity was determined by dividing the percentage of GFP-positive cells in Sce-I transfected cells by the basal percentage of GFP signal in mock control.

siRNA screening

The siRNA targeting reagents were purchased from Dharmacon, as a SMARTpool of four distinct siRNA species targeting different sequences of the target transcript. Cell lines were grown and transfected with SMARTpool siRNAs using RNAiMAX (Invitrogen) transfection reagents following manufacturer's instructions. Briefly, RNAi screening conditions were as follows: on day one, siRNA were distributed in each well of a 6-well plate at the final concentration of 20 nmol/L. Transfection reagents were diluted in OptiMEM and aliquoted at 250µl/well. After 20 minutes of incubation, 2ml of cells in media without

antibiotics were added to each well. After 72 hours, cells were analyzed by Western blot. AllStars (Qiagen) non-targeting siRNA was used as negative control.

Generation of patient derived xenografts

Patient tumor sample was obtained under the approval of the local Ethical committee of the institution and of the Italian Ministry of Health. To perform animal experiments on PDXs (patient-derived xenografts), tumor specimens were subcutaneously propagated in NOD-SCID mice (Charles River Laboratory). When tumors reached nearly 300 mm^3 in volume, cetuximab (Merck, 10 mg/kg) was administered twice/week by intraperitoneal injection. Tumor size was evaluated weekly by caliper measurements, and the volume of the mass was calculated using the formula V = (d2×D)/2 (d = minor tumor axis; D = major tumor axis) and reported as tumor mass volume (mm^3). Animal procedures were approved by the Ethical Commission of the Candiolo Cancer Institute and by the Italian Ministry of Health.

CRISPR/Cas9 *MLH1* knock-out

To generate the *MLH1* knock-out, we used the genome editing one vector system (lentiCRISPR-v2) (Addgene plasmid: 52961). Small guide RNAs (sgRNAs) were designed using the CRISPR tool (http://crispr.mit.edu). Annealed sgRNA oligonucleotides targeting the human *MLH1* gene were cloned into Bsmbl lentiCRISPR-v2 plasmid as previously described(*52*). For transient expression of CRISPR-Cas9 system, cells were transfected with lentiCRISPR-v2 vector plasmid. Transfection was carried out using Lipofectamine 3000 (Life technologies) and OptiMEM (Invitrogen), according to the manufacturer's instructions. After 48 hours, cells were incubated with puromycin (Sigma Aldrich) for 4 days and subsequently single cell diluted in 96-well plates. Two independent clones (cl.1 and cl.2) were selected and loss of MLH1 protein expression and absence of Cas9 were confirmed by Western blot. HT29 cells transfected with non-targeting (empty) sgRNA were used as control.

ROS production assay

DiFi and WiDr parental and derivative resistant cells were seeded in 96-well white-walled plates (12×10^3 cells/well for DiFi and 6×10^3 cells/well for WiDr) and incubated overnight for attachment. The following day, cells were treated as follow: 50 µg/ml cetuximab for DiFi; 1 µM dabrafenib + 20 µg/ml cetuximab for WiDr. After 48, 72, and 96 hours ROS were measured by ROS-Glo™ H2O2 Assay (Promega) according to the manufacturer's protocol. Luminescence was measured using a plate-reading luminometer (TECAN Spark 10M) and the resulting data were normalized to untreated cells at each time point. The antioxidant N-acetyl-cysteine (NAC, Sigma) was used at the final concentration of 10 mM as a control for the rescue experiment.

RNAseq data analysis

Prior to analysis, cells were grown in their specific media supplemented with 10% FBS and treated as follow: 100µg/ml of cetuximab (CTX) for DiFi; 50µg/ml cetuximab (CTX) +1µM dabrafenib (DAB) for WiDr.

Total RNA was extracted using Maxwell® RSC miRNA Tissue Kit (AS1460, Promega), according to the manufacturer's protocol. The quantification of RNA was performed by DS-11 Spectrophotometer (DeNovix) and Qubit 3.0 Fluorometer (Life Technologies).
RNA integrity was evaluated with the Agilent 2100 Bioanalyzer using the Agilent RNA 6000 Nano Kit. Total RNA (500 ng) with RNA integrity number (RIN) score between 9 and 10 was used as input to the Illumina TruSeq RNA Sample Prep Kit v2-Set A and B (48Rxn), according to the manufacturer's protocol.
The standard RNA fragmentation profile was used (94 °C for 8 min for the TruSeq RNA Sample Prep Kit). RNA-seq library quality was assessed using the Agilent DNA 1000 kit on the Agilent 2100 BioAnalyzer and quantified using Qubit 3.0 Fluorometer (Life Technologies). Libraries were diluted to 10 nM using Tris-HCl (10 mM pH 8.5) and then pooled together. Diluted pools were denatured according to the standard Illumina protocol.
FastQ files produced by Illumina NextSeq500 were aligned using MapSplice2 (*53*) transcriptome-aware aligner using hg38 assembly as reference genome. The resulting BAM files were post-processed to translate genomic coordinates to transcriptomic ones and to filter out alignments carrying insertion or deletions or falling outside the transcriptome regions. The post-processed BAM alignment was given as input to RSEM (*54*) for gene expression quantification using GENCODE (*55*) v22 as gene annotation.

Whole exome sequencing and mutational burden calculation
Library preparation, enrichment of whole exome regions, and sequencing were performed by Integragen SA (Evry, France) according to standard protocols (*56*). Bioinformatic analysis was performed as previously reported (*57*). The FASTQ sequence files were pre-processed to remove adapter sequences using "agilentreadtrimmer" and were then mapped to the human genome version 19 (hg19) using BWA-mem algorithm. For PDX samples, mouse-derived reads were distinguished by human reads and removed using XENOME (*58*). PCR duplicates were removed using the RMDUP command of SAMtools package. The median depth for each sample is reported in Table S1. Targeted regions covered by at least 40 reads were between 87.6% and 95.1%. The mutational burden (MB) was calculated from WES data taking into consideration nucleotide variants supported by a minimum of 4 mutated reads in regions with a minimum depth of 5X. We considered only mutations with allele frequency higher than 10%, excluding mutations annotated in dbSNP (v147) and somatic mutations relevant in cancer annotated in COSMICdb (v75). All data were also normalized on specific covered target regions.

Analysis of homopolimer and microsatellite genomic regions
The overall bioinformatic approach is based on previously published literature (*59*). Specifically, the reference genome (human genome version 19) was analyzed to identify homopolimer and microsatellite genomic regions up to five nucleotides in length and with at least five consecutive repeats. A total of 33,386,402 regions were identified. Using WES data, reads located in one of the identified regions were extracted. Regions with less than 20 encompassing reads in one of two paired samples were discarded. At least 11,000 regions for each pair were included in the analysis. Read lengths of pre- and post-therapy

samples were measured, and the distribution for each sample pair was calculated. Next, a standard $\chi 2$ test was performed for each region (pre- and post-therapy). A region was considered unstable when the $\chi 2$ p-value was less than 0.05. The percentage of unstable regions is defined as the ratio between the number of unstable regions and the total number of regions included in the analysis for each pair.

NGS high depth capture panel

The NGS high depth capture panel is designed on hotspots of 42 target genes relevant for colorectal cancer. The genomic size is 55 kilobases for a total of 300 captured regions. All coding sequences of all isoforms of 8 clinical relevant genes are included: *APC, BRAF, ERBB2*, *MET*, *TP53* and MMR pathway genes (*MLH1, MSH2* and *MSH6*). The target panel is characterized by the presence of tandem repeats sequences (5 loci) useful to determine the stability of microsatellite regions (MSI status). A list of 54 single-nucleotide polymorphisms (SNPs) was used to identify the allelic profile and to build the single-nucleotide polymorphism identifier (SNP_ID) of each sample. The regions captured are reported in Table S2. Libraries preparation methods optimized for analysis of small targets were applied (*60, 61*).

Statistical Analyses

Statistical significance was determined by two-tailed Student's t-test or TwoWay ANOVA (GraphPad Prism) as specified for each experiment and $p < 0.05$ was considered statistically significant.

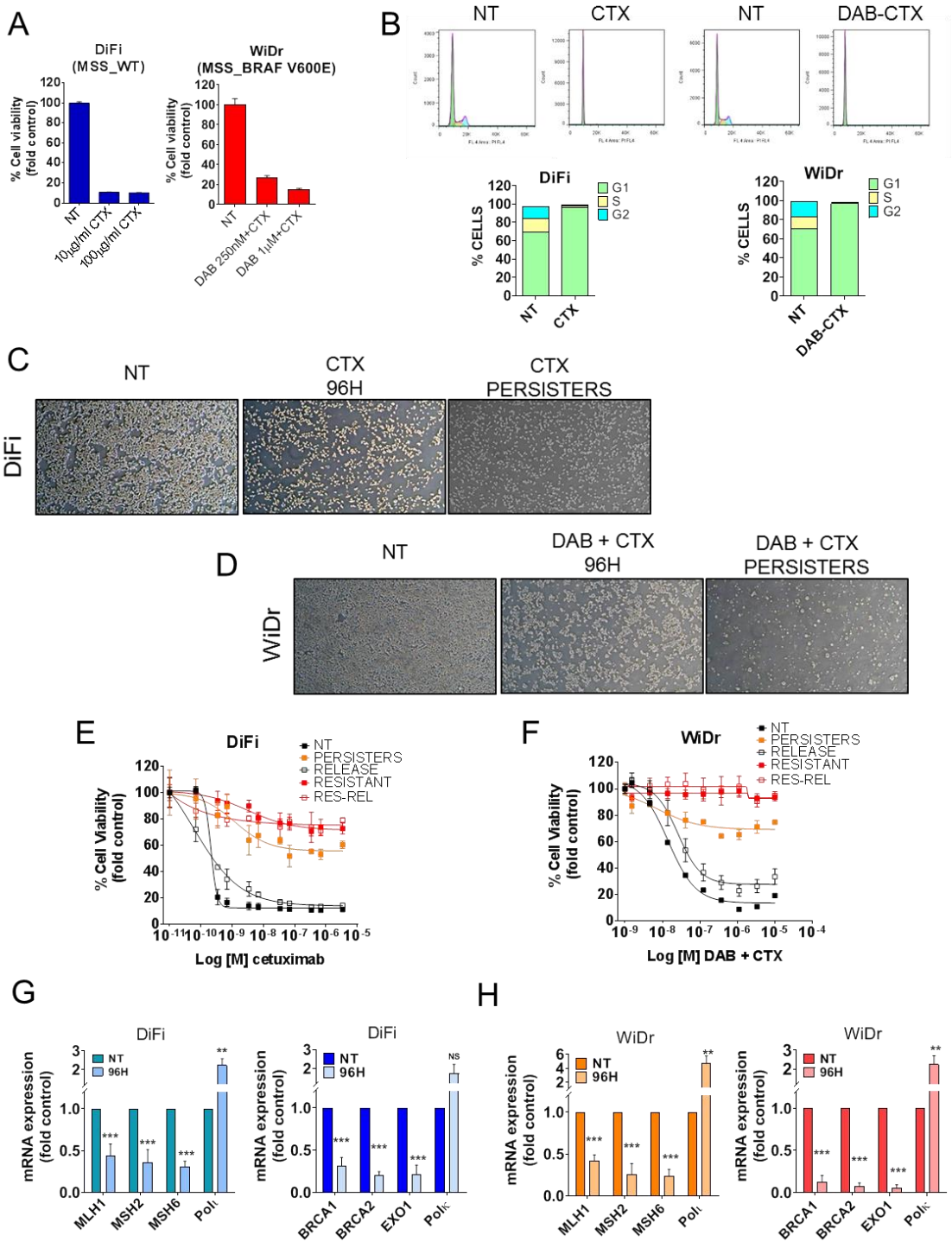
A
DiFi
(MSS_WT)
WiDr
(MSS_BRAF V600E)
% Cell viability
(fold control)
NT
10µg/ml CTX
100µg/ml CTX
DAB 250nM+CTX
DAB 1µM+CTX
B
NT
CTX
NT
DAB-CTX
DiFi
WiDr
% CELLS
G1
S
G2
C
NT
CTX
96H
CTX
PERSISTERS
DiFi
D
NT
DAB + CTX
96H
DAB + CTX
PERSISTERS
WiDr
E
DiFi
NT
PERSISTERS
RELEASE
RESISTANT
RES-REL
% Cell Viability
(fold control)
Log [M] cetuximab
F
WiDr
NT
PERSISTERS
RELEASE
RESISTANT
RES-REL
% Cell Viability
(fold control)
Log [M] DAB + CTX
G
DiFi
NT
96H
mRNA expression
(fold control)
MLH1
MSH2
MSH6
Polι
BRCA1
BRCA2
EXO1
Polκ
NS
H
WiDr
NT
96H
mRNA expression
(fold control)
MLH1
MSH2
MSH6
Polι
BRCA1
BRCA2
EXO1
Polκ

Fig. S1. Cell cycle arrest, generation of persister cells and alteration of DNA repair genes in CRC cells treated with targeted agents. (A) DiFi and WiDr cells were treated as indicated for 96 hours. Cell viability was assayed by the ATP assay. Bars represent means ± SD of three technical replicates. (B) DiFi and WiDr cell lines were treated with 50μg/ml cetuximab alone (DiFi) or in combination with 1μM dabrafenib (DAB) (WiDr). Untreated cells (NT) were used as control. Ninety-six hours later, cells were analyzed by flow cytometry. Distribution of cells in G1, S and G2 phases is reported in the bar graph. (C-D) DiFi cells were treated with 100μg/ml of cetuximab (CTX), and WiDr were treated with 50μg/ml cetuximab + 1μM dabrafenib (DAB) for 96h or for 2 weeks (PERSISTERS). Representative cells images are shown. NT, untreated control cells. (E-F) DiFi and WiDr cells were treated for 2 weeks with cetuximab (CTX) alone or in combination with dabrafenib, respectively, till drug-tolerant cells survived (PERSISTERS). Cells were then either released from drug pressure (RELEASE) or continuously treated until resistance arose (RESISTANT). After that, viability of resistant cells upon drug withdrawal (RES-REL) was further measured. NT, untreated control parental cells. (G-H) Ninety-six hours after administration of cetuximab (DiFi) or cetuximab + dabrafenib (WiDr) the expression of the indicated genes was evaluated by RT-PCR. Results represent means ± SD of at least 3 independent experiments. **p< 0.01; ***p< 0.001 (Student's t test). NS, not statistically significant differences.

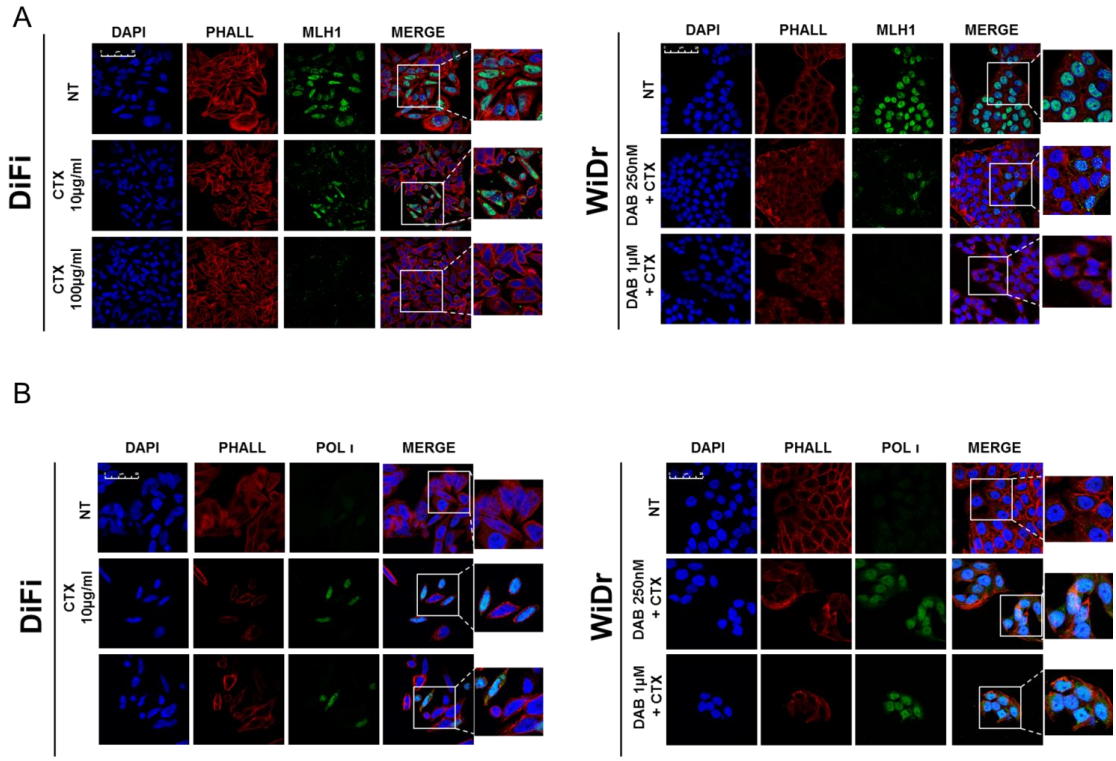

Fig. S2. Alteration of DNA repair in CRC cells. (A) CRC cells were treated for 72 hours as indicated. After that cells were fixed and stained. Vehicle-treated cells (NT) were used as control. Nuclei were stained with DAPI (blue) and anti-MLH1 antibody (green). Actin was stained with Phalloidin (red). Scale bar: 25μm. Representative images of each condition are shown. (B) CRC cells were treated for 72 hours as reported. After that cells were fixed and stained. Vehicle-treated cells (NT) were used as control. Nuclei were stained with DAPI (blue) and anti-Polι antibody (green). Actin was stained with

Phalloidin (red). Scale bar: 50μm. Representative images of each condition are reported. DAB, dabrafenib; CTX, cetuximab.

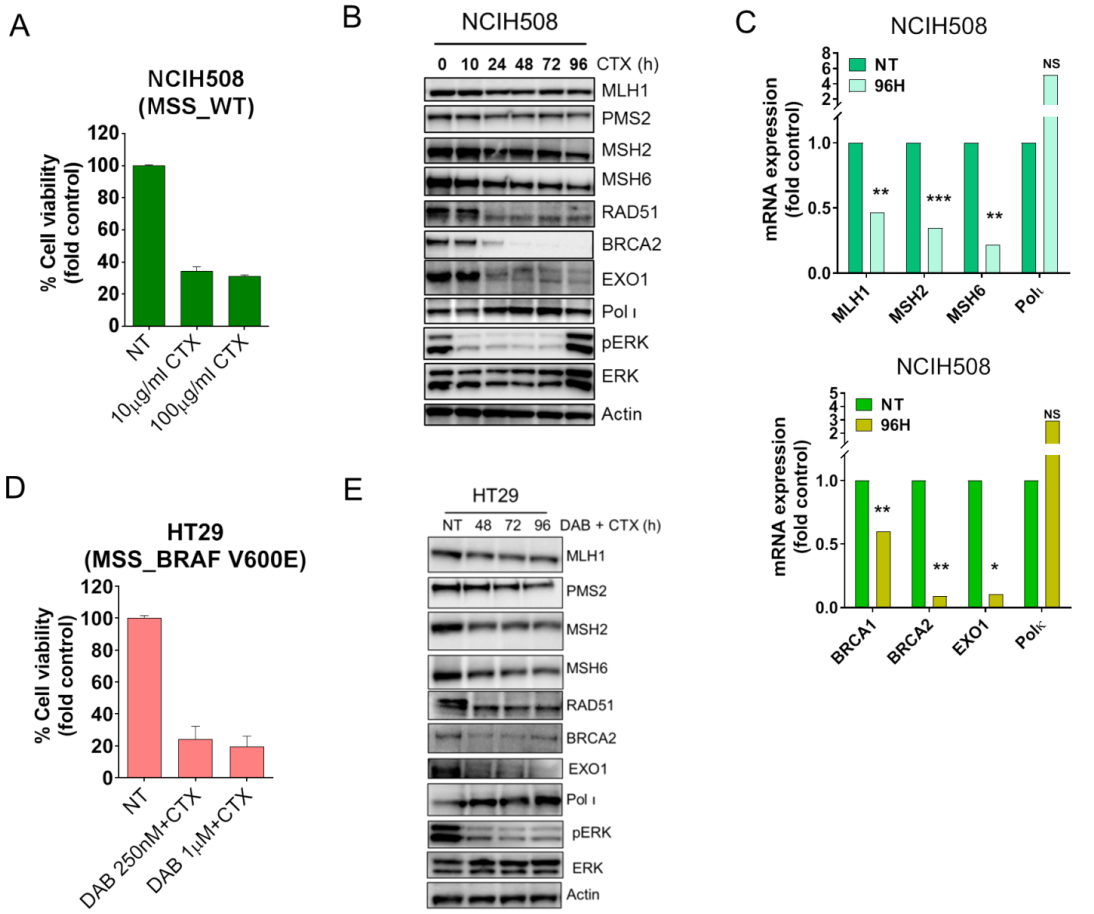

Fig. S3. Down-modulation of MMR and HR genes in CRC cells sensitive to targeted therapies. (A) NCIH508 cells were treated with the indicated concentration of cetuximab for 96h. Cell viability was assayed by ATP assay. Bars represent means ± SD of three technical replicates. (B) NCIH508 cells were treated and analyzed at indicated time points by Western blot. (C) Ninety-six hours after cetuximab administration, the expression of the indicated genes was evaluated by RT-PCR. Bars represent means of two independent experiments. *p < 0.05; **p< 0.01; ***p< 0.001 (Student's t test). NS, not statistically significant differences. (D) HT29 cells were treated with indicated therapeutic regimens for 96h. Cell viability was measured by ATP assay. Bars represent means ± SD of three technical replicates. (E) HT29 cells were treated and analyzed at indicated time points by Western blot. DAB, dabrafenib; CTX, cetuximab. NT, untreated cells.

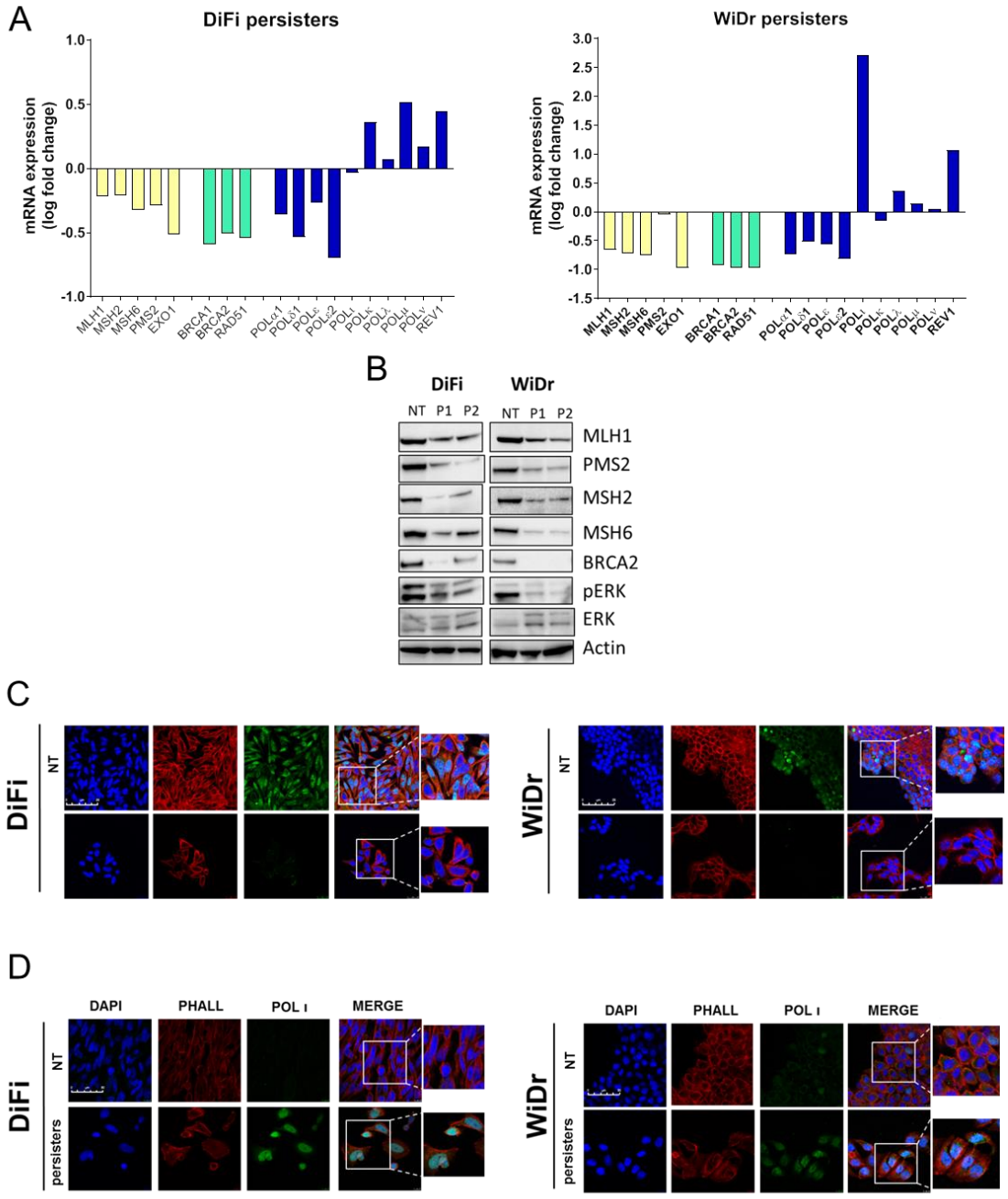

Fig. S4. Analysis of DNA repair effectors in persisters cells. (A) DiFi and WiDr cells were treated for 2 weeks until the persister state was reached and RNAseq analysis was then performed. Mismatch repair (MMR) (yellow), homologous recombination (HR) (green), and DNA polymerases (blue) genes are reported. Results represent means of two independent experiments. (B) Expression levels of MMR and HR DNA repair proteins were evaluated in 2 independent persister populations (P1 and P2) for each cell line model. NT stands for untreated cells. (C) Persisters cells and vehicle-treated cells (NT) were fixed and stained. Nuclei were stained with DAPI (blue) and anti-MLH1 antibody (green). Actin was stained with Phalloidin (red). Scale bar: 25μm. Representative images of each condition are reported. (D) Persisters cells and vehicle-treated cells (NT) were fixed and stained. Nuclei were stained with DAPI (blue) and anti-

Polι antibody (green). Actin was stained with Phalloidin (red). Scale bar: 50μm. Representative images of each condition are reported.

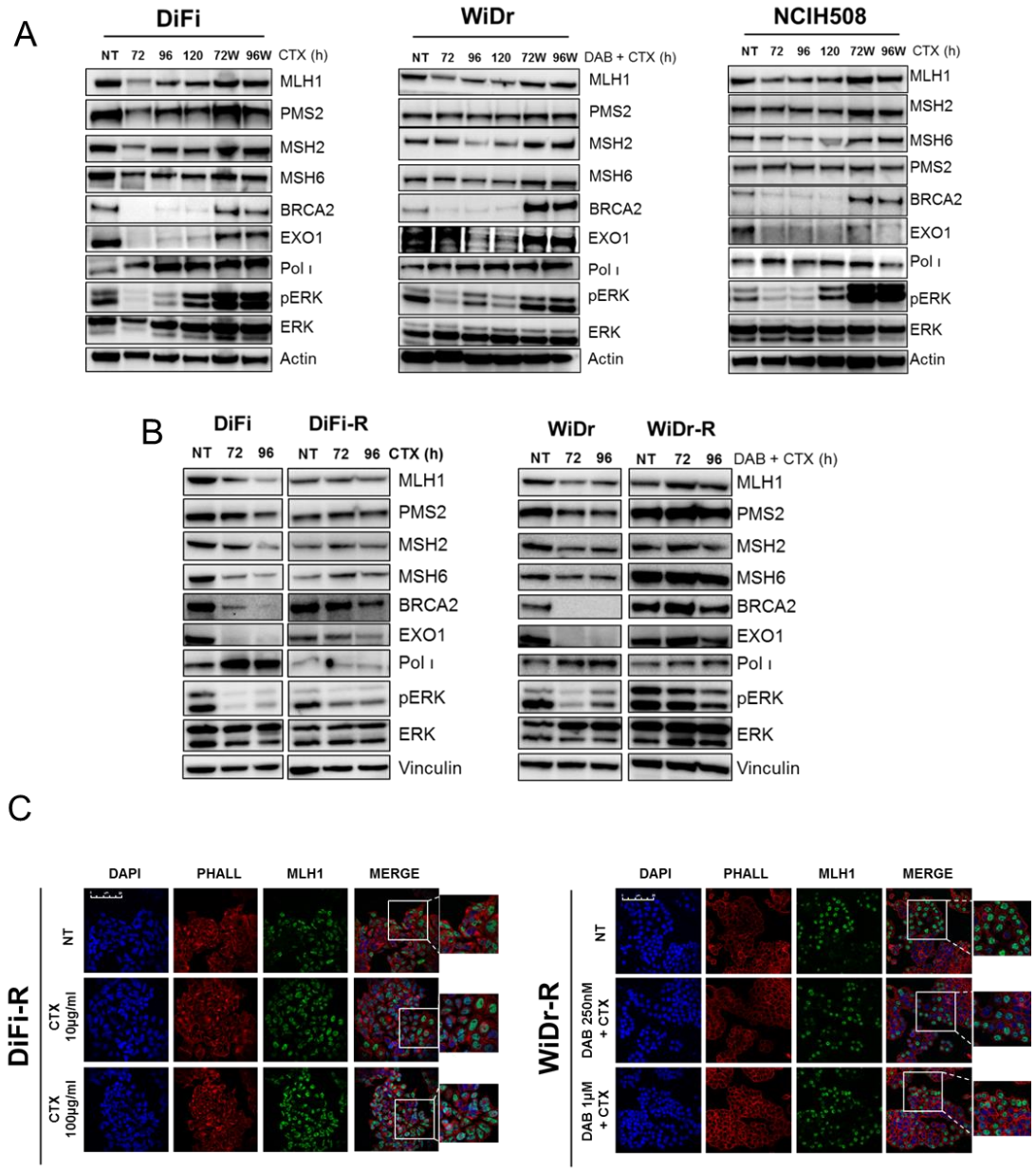

Fig. S5. Transient modulation of DNA repair proteins by drug treatment. (A) Modulation of DNA repair proteins was measured upon withdrawal of targeted therapies. The indicated parental cells were treated with either cetuximab (CTX) alone (DiFi and NCIH508) or in combination with dabrafenib (DAB) (WiDr) for 72, 96, and 120 hours. Treatment was then removed for additional 72 (72W) or 96 (96W) hours and protein expression was analyzed by Western blot. (B) DiFi and WiDr parental and permanently resistant (-R) derivatives were treated with 50µg/ml of cetuximab (CTX) alone or in combination with 1µM dabrafenib (DAB) and protein expression was analyzed by Western blot. (C) Ninety-six hours after indicated drugs treatment, resistant cells were fixed. Cells were stained with DAPI (blue-nuclei) and anti-MLH1 antibody (green). Actin was stained with Phalloidin (red). Scale bar: 25µm. Representative images of each condition are reported. NT, untreated cells.

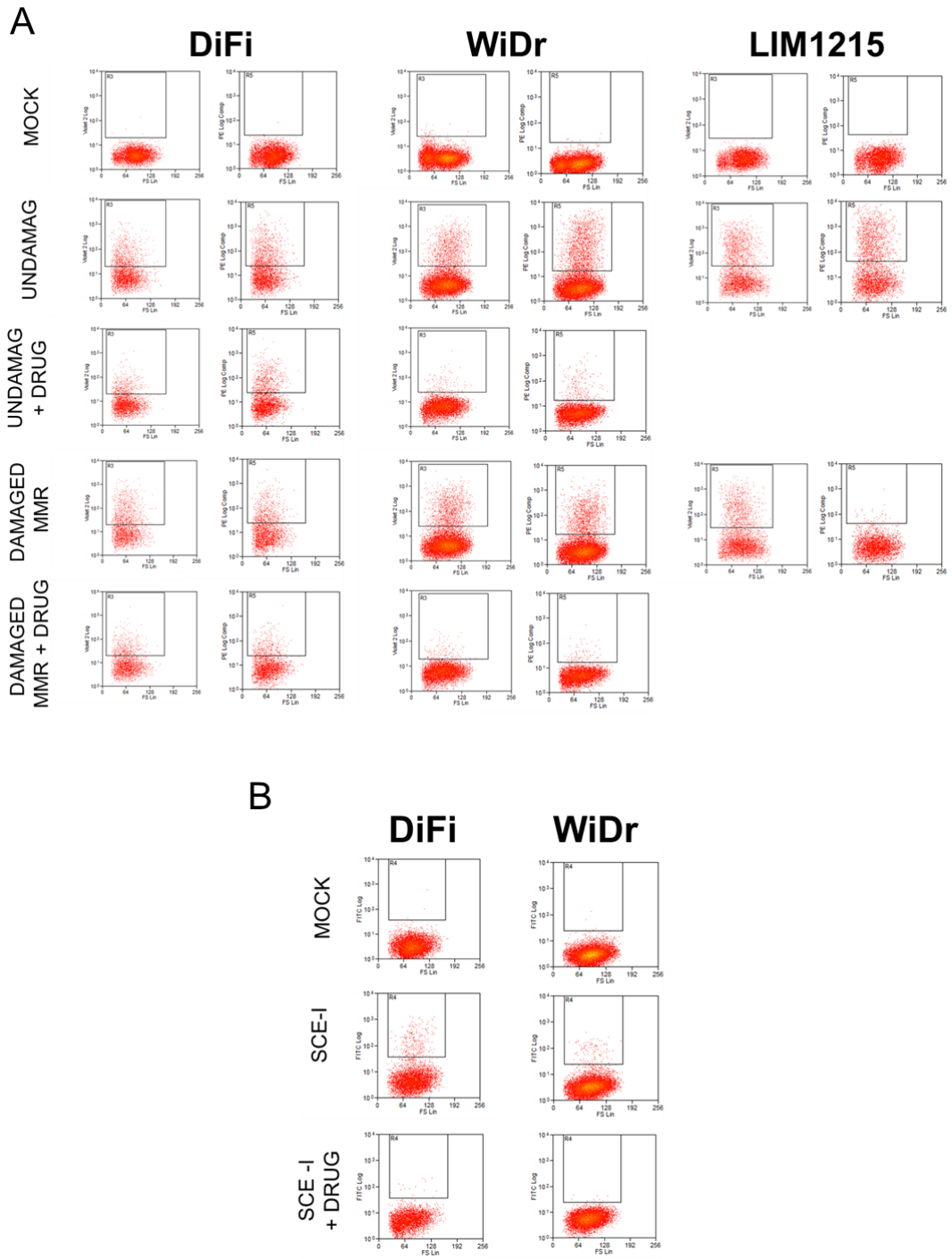

Fig. S6. Drugs targeting EGFR and BRAF influence MMR and HR capabilities of CRC cells. (A) The indicated CRC cells were transfected with G:C undamaged plasmid or with G:G mismatch-damaged (MMR) plasmid. Where indicated (DRUG), cells were treated with targeted therapies for fifty-sixty hours and analyzed by flow cytometry. A mock transfection was used as control. The pmax-BFP (VIOLET channel) was used as internal control for transfection efficiency to normalize the mOrange (PE channel) signal. MMR deficient CRC cells LIM1215 were used as a positive control for MMR loss. Results of one representative experiment are reported. (B) pDRGFP-stably expressing CRC cells were transfected with the pCBASce-I plasmid and then either left in the absence of drug or treated with targeted therapies (DRUG) for fifty-sixty hours and analyzed by flow cytometry. A mock transfection was used as control. Results of one representative experiment are reported.

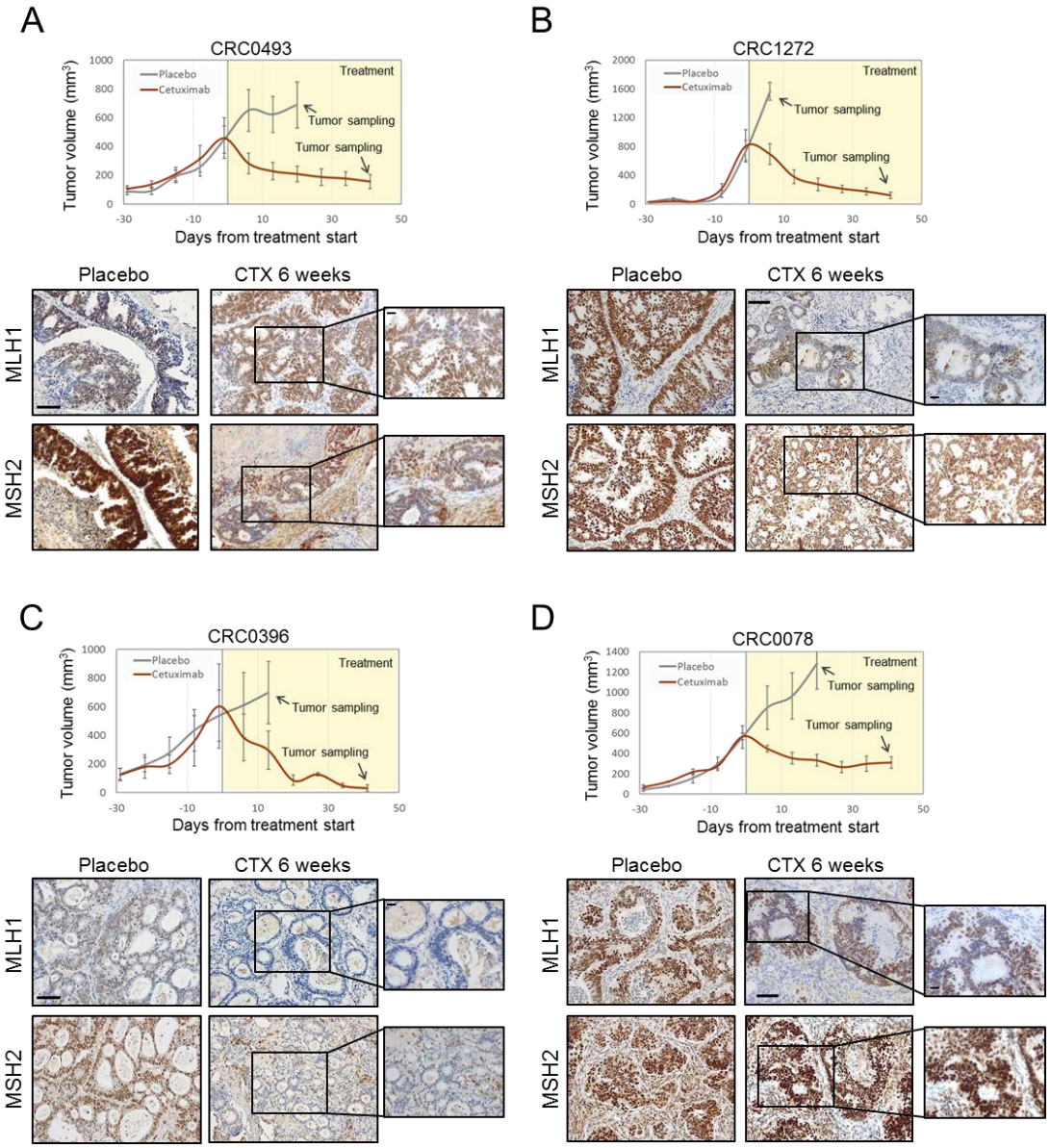

Fig. S7. Altered expression of MMR proteins in PDXs treated with cetuximab. (A-D) Tumor regression in the indicated PDX models after treatment with cetuximab (CTX) (20 mg/kg twice weekly) for 6 weeks. Growth curve kinetics are shown in the upper panels. Mean tumor volumes ± SEM are shown (*n* = 6 mice per treatment arm). Immunohistochemical analysis with anti-MLH1 and anti-MSH2 antibodies of histologic tumor sections derived after 6 weeks of cetuximab administration are shown in the lower panels. Tumor sections derived from placebo arm were used as control. Scale bar 0.1mm. Magnifications ×40 (scale bar 0.05mm).

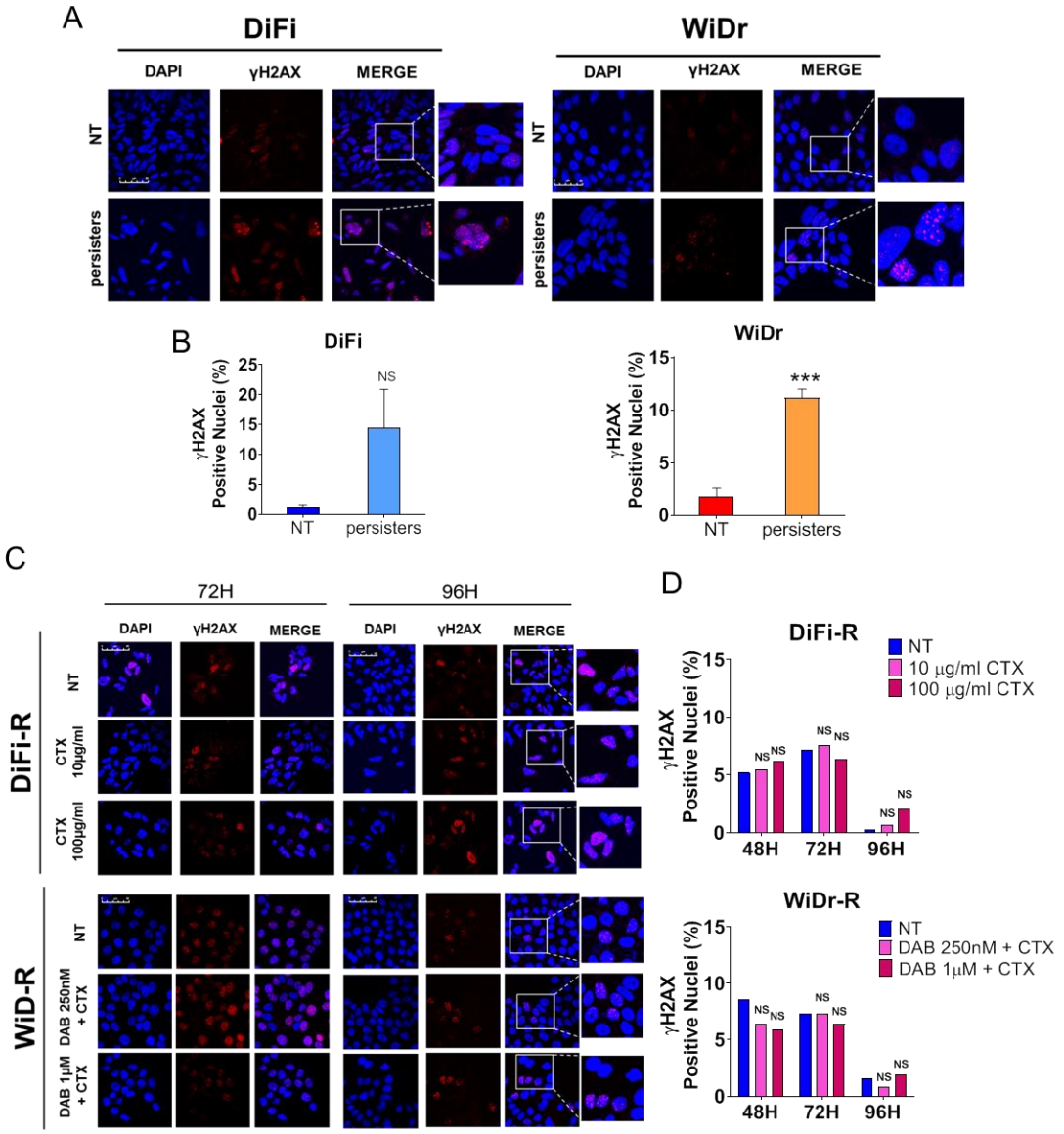

Fig. S8. Monitoring DNA damage in persisters and resistant CRC cells. (A) DiFi (left) and WiDr (right) persisters cells and vehicle-treated control (NT) were fixed and stained. Nuclei were stained with DAPI (blue) and anti-γH2AX antibody (red). Scale bar: 50μm. Representative images of each condition are shown. (B) Quantitation of nuclear γH2AX foci in DiFi and WiDr untreated (NT) and persisters cells. Nuclei with five or more γH2AX foci were scored as positive, and at least 500 nuclei were counted for each sample. Results represent means ± SD (n=3). ***p <0.001 (Two Way Anova). NS, not statistically significant differences. (C) Resistant CRC cells (-R) were treated as indicated. After indicated time points, cells were fixed and stained. Vehicle-treated cells (NT) were used as control. Nuclei were stained with DAPI (blue) and anti-γH2AX antibody (red). Scale bar: 50μm. Representative images of each condition are shown. (D) Quantitation of nuclear γH2AX foci in DiFi resistant (upper panel) and WiDr resistant (lower panel) untreated or treated cells. Nuclei with five or more γH2AX foci were scored as positive, and at least 500 nuclei were counted for each sample. Results represent means of two independent experiments. NS, not statistically significant differences. DAB, dabrafenib; CTX, cetuximab.

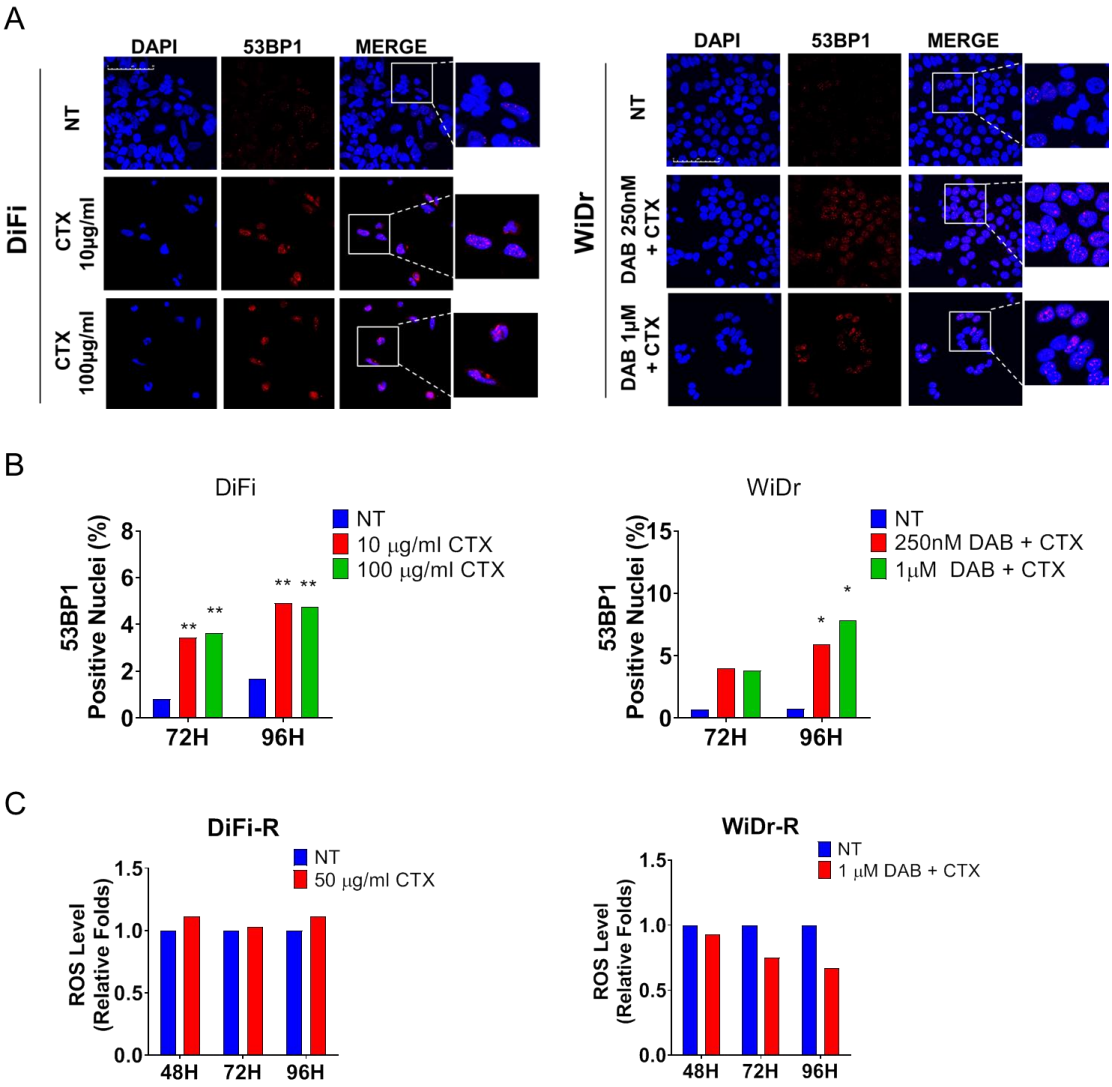

Fig. S9. Drug-induced switch from HR to NHEJ-mediated DSB repair. (A) Detection of 53BP1 foci in the indicated CRC cells. Vehicle-treated cells (NT) were used as control. Cells were fixed and stained after 72 hours of treatment. Nuclei were stained with DAPI (blue) and anti-53BP1 antibody (red). Scale bar: 50µm. Representative images for each condition are shown. (B) Quantification of nuclear 53BP1 foci in DiFi and WiDr cells after indicated treatment schedules. Nuclei with five or more 53BP1 foci were scored as positive and at least 500 nuclei were counted for each sample. Results represent means of two independent experiments. *p<0.05; **p< 0.01 (Two Way ANOVA). DAB, dabrafenib; CTX, cetuximab. (C) Resistant cells (-R) were treated with 50µg/ml of cetuximab (DiFi) or 20µg/ml cetuximab + 1µM dabrafenib (WiDr) and ROS levels were measured. Results represent means of two independent experiments. DAB, dabrafenib; CTX, cetuximab.

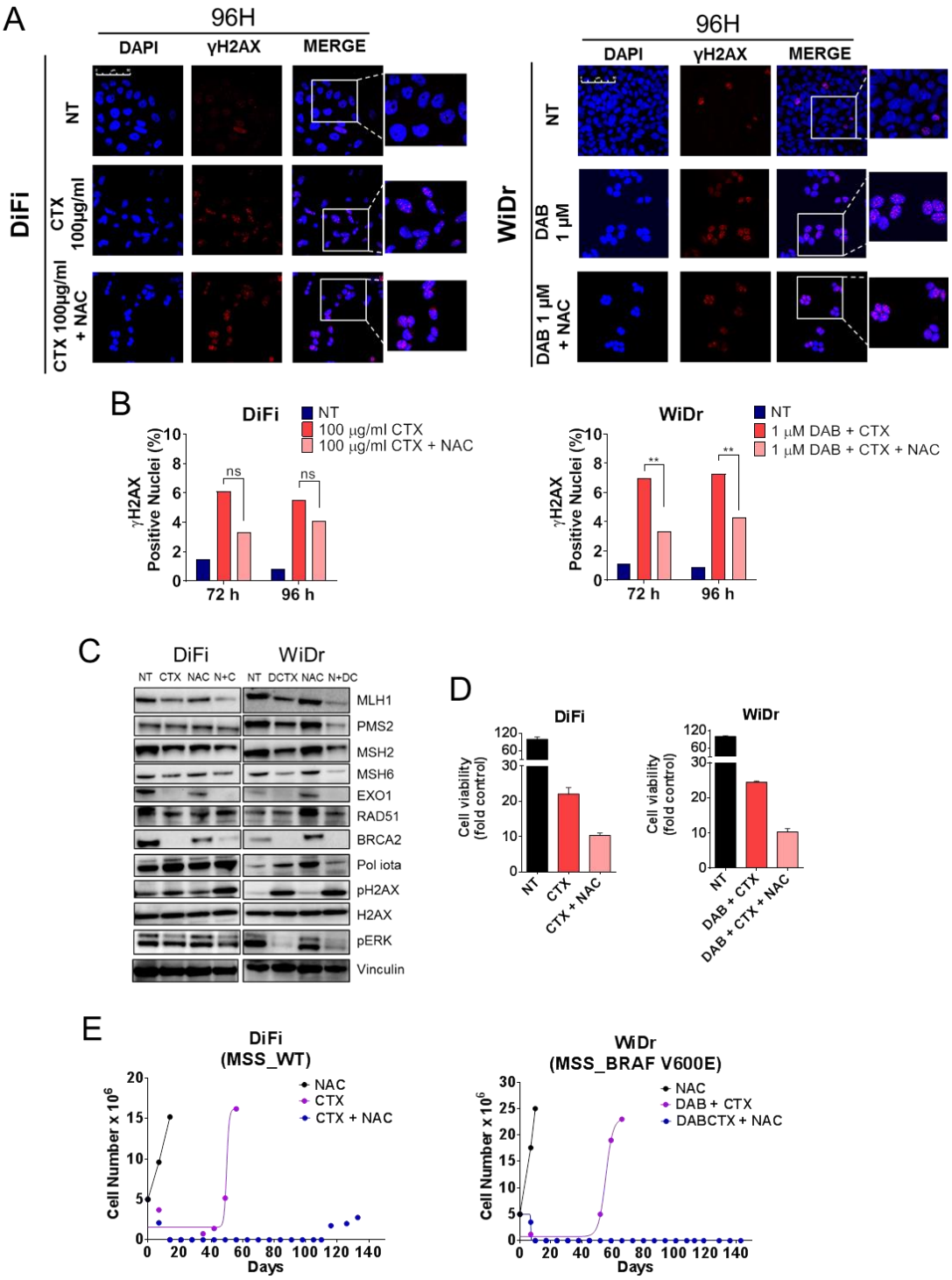

Fig. S10. Effect of ROS modulation on CRC cells treated with targeted therapies. (A) Detection of γH2AX foci in the indicated CRC cells. Vehicle-treated cells (NT) were used as control. Cells were fixed and stained at indicated time points. Nuclei were stained with DAPI (blue) and anti-γH2AX antibody (red). Scale bar: 50µm. Representative images for each condition are shown. (B) Quantification of nuclear γH2AX foci in DiFi (left panel) and WiDr (right panel) cells after indicated treatment schedules. Nuclei with five or more γH2AX foci were scored as positive and at least 500 nuclei were counted for each sample. Results represent means of two independent experiments. **p< 0.01 (Two Way ANOVA). NS, not statistically significant differences. DAB, dabrafenib; CTX,

cetuximab. (C) CRC cells were treated with 100µg/ml cetuximab (CTX) (DiFi), 50µg/ml cetuximab + 1µM dabrafenib (DCTX) (WiDr), 10mM NAC or their combinations (N+C; N+DC) for 72 hours. Cell protein lysates were analyzed by Western blot. NT, untreated control cells. (D) CRC cells were treated with cetuximab (CTX), dabrafenib + cetuximab (DAB + CTX), NAC their combinations for 5 days. Cell viability was assayed by the ATP assay. Bars represent means ± SD of three technical replicates. (E) BRAF-mutated WiDr cells and *RAS*/*RAF* WT DiFi were treated with 10mM NAC alone, MAPK pathway inhibitor(s) or combination of both until secondary resistance emerged. DAB, dabrafenib; CTX, cetuximab.

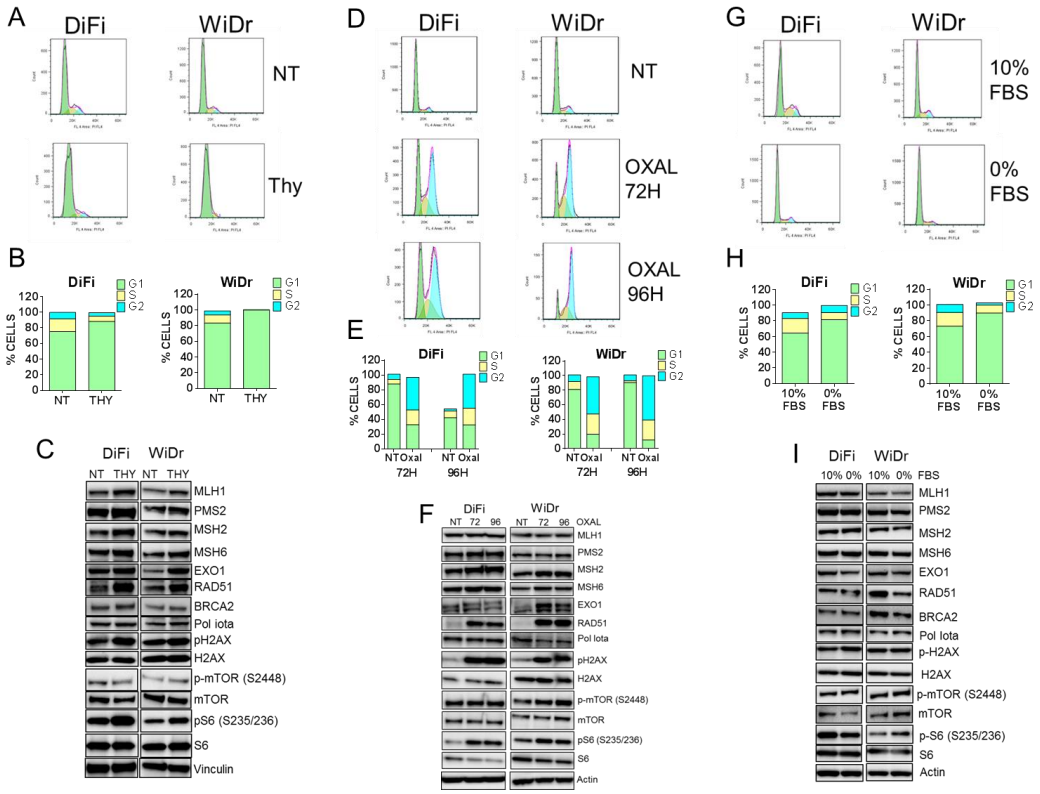

Fig. S11. Impact of different types of stress on CRC cells. (A) DiFi and WiDr cell lines were treated with two cycles of thymidine (THY) administration and, after that, cells were analyzed by flow cytometry. (B) Distribution of cells in G1, S and G2 phases upon double-block with thymidine (THY). (C) Western blot analysis of MMR and HR proteins upon double-block with thymidine (THY). (D) DiFi and WiDr cell lines were treated with 10µM oxaliplatin (OXAL) and, after that, cells were analyzed by flow cytometry. (E) Distribution of cells in G1, S and G2 phases upon oxaliplatin treatment at indicated time points. (F) CRC cells were treated with 10µM oxaliplatin (OXAL) for 72 and 96 hours, after that protein lysates were analyzed by Western blot. NT, untreated cells. (G) DiFi and WiDr cell lines were grown in medium without serum (0% FBS) for 24 hours; after that, cells were analyzed by flow cytometry. Cells grown in standard culturing conditions (10% FBS) were used as control. (H) Distribution of cells in G1, S and G2 phases after 24 hours in standard culture conditions (10% FBS) or upon serum

starvation (0% FBS). (I) CRC cells were cultured for 24 hours in 10% FBS or in 0% FBS media and analyzed by Western blot.

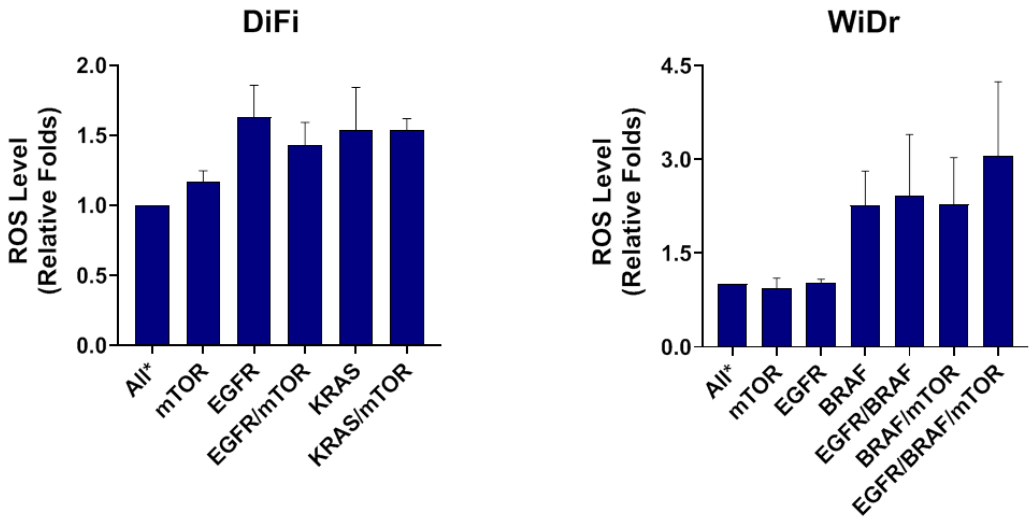

Fig. S12. Silencing of driver oncogenes triggers ROS induction in CRC cells WT DiFi and *BRAF* p.V600E-mutated WiDr cells were transfected with the indicated siRNAs or combinations of them. Seventy-two hours after siRNA transfection ROS levels were measured. Results represent means ± SD (n=3). All*, non-targeting siRNA.

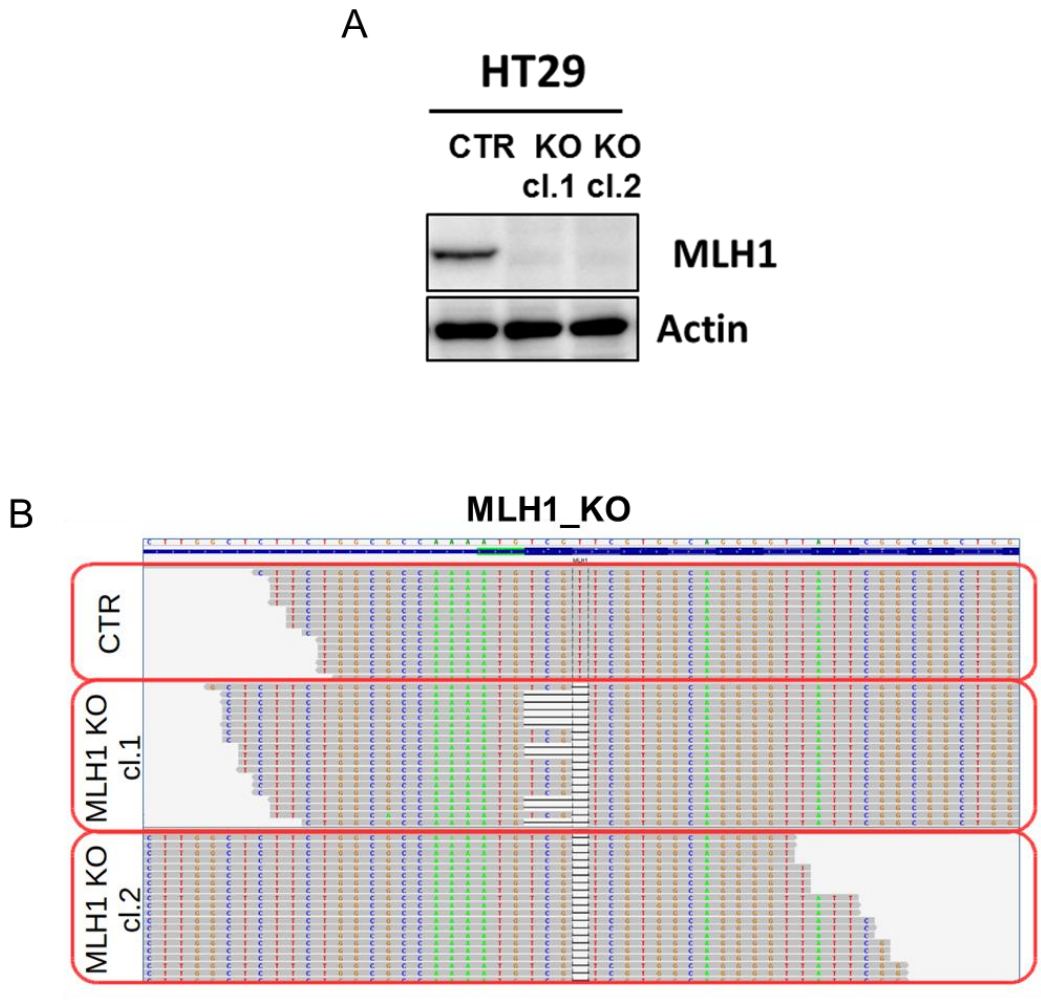

Fig. S13. Knock-out of the *MLH1* gene in HT29 CRC cells. (A) CRISPR/CAS9-mediated knock-out (KO) of *MLH1* gene in HT29 CRC cells was validated at the protein level. CTR stands for control cells (with intact *MLH1* gene); cl.1 and cl.2 are two independent *MLH1*-KO clones. (B) Exome sequencing data were used to identify molecular alterations in the *MLH1* gene in the genome-edited HT29 cells. Alignment of sequence reads harboring deletions of the *MLH1* gene after gene editing is shown. The upper sequence corresponds to the human reference assembly hg19. CTR stands for control cells (with intact *MLH1* gene); clone 1 carries heterozygous deletions (1 base pairs and 4 base pairs) that induced frameshifts (100%); clone 2 carries a homozygous deletion that produced a frameshift (100%).

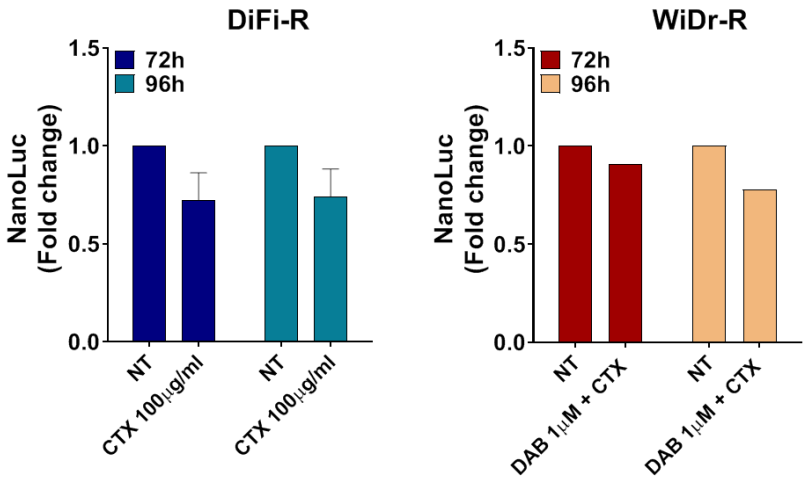

Fig. S14. Mutagenic assays in drug-resistant CRC cells. CRC resistant (-R) cells were treated with the indicated therapeutic regimens. NanoLuc signal from treated and untreated (NT) resistant cells was normalized to cell viability. NanoLuc signal from treated cells was compared to untreated (NT) cells. Results represent means ± SD (n=4 for DiFi; n=2 for WiDr).

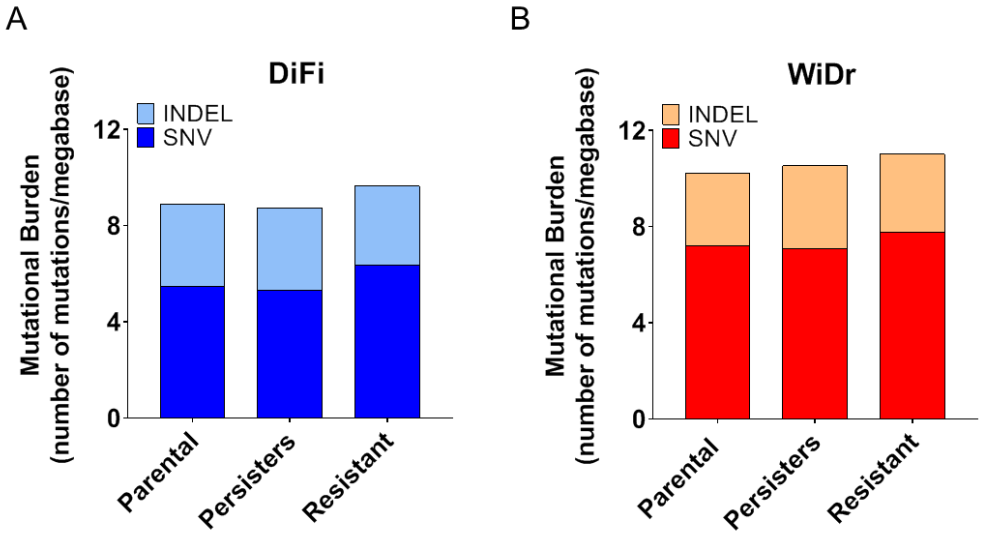

Fig. S15. Whole exome sequencing analysis of CRC cells upon drug-induced stress. Mutational burden (number of mutations/megabase) was measured using whole exome sequencing data in DiFi (A), and WiDr (B) cells. Only mutations with allele frequency above 10% were considered. Mutations annotated as SNP in dbSNP (v147) and somatic mutations relevant in cancer and annotated in COSMICdb (v75) were filtered out. Insertion/deletions (INDEL) and Single Nucleotide Variations (SNV) are reported. Data were normalized on the specific covered target region of each WES.

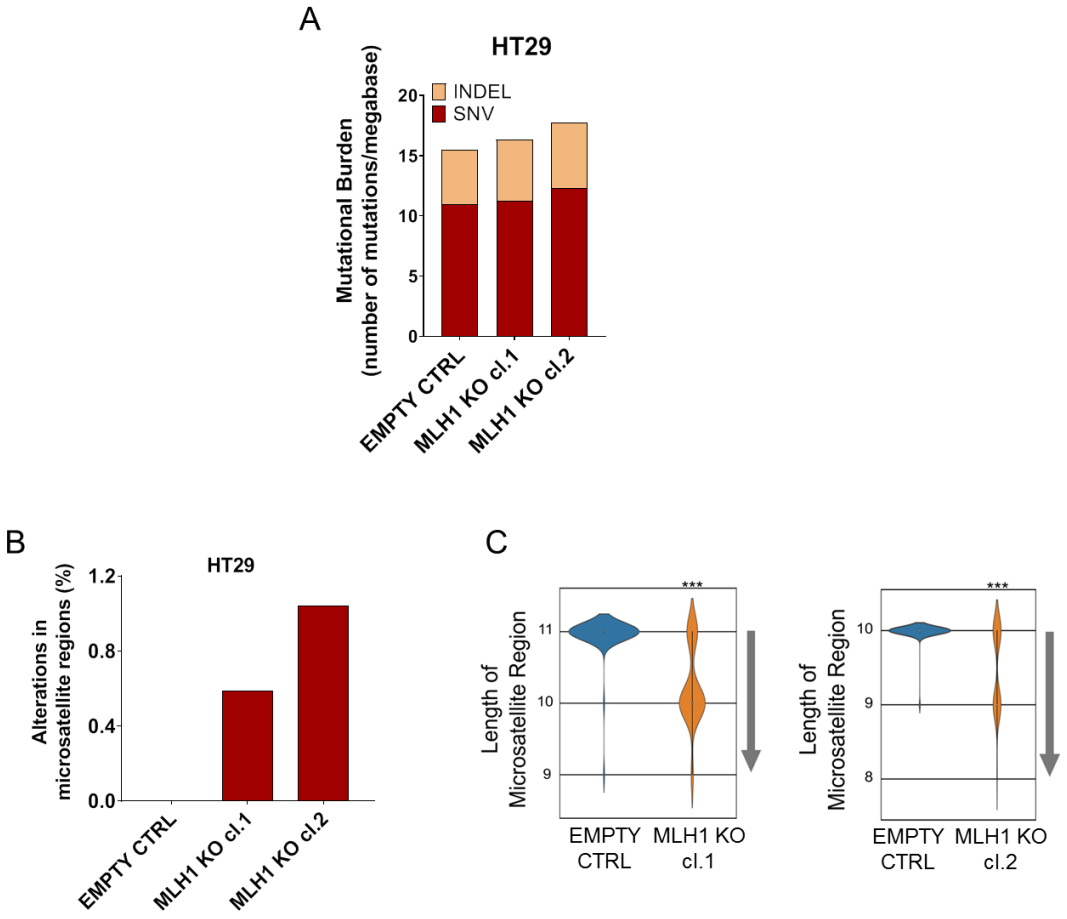

Fig. S16. Molecular landscape of CRC cells upon genetic disruption of the *MLH1* gene. (A) Mutational burden (number of mutations/megabase) was measured using whole exome sequencing data. Only mutations with allele frequency above 10% were considered. Mutations annotated as SNP in dbSNP (v147) and somatic mutations relevant in cancer and annotated in COSMICdb (v75) were filtered out. Insertion/deletions (INDEL) and Single Nucleotide Variations (SNV) are reported. Data were normalized on the specific covered target region of each WES. (B) Percentage of unstable microsatellite regions in *MLH1*-KO cells clone 1 (cl.1) and clone 2 (cl.2) compared to their parental counterpart (EMPTY CTRL). (C) Lengths distribution of one representative microsatellite region for HT29 *MLH1*-KO clone 1 and clone 2 is reported. ***$p < 0.001$ ($\chi 2$ test).

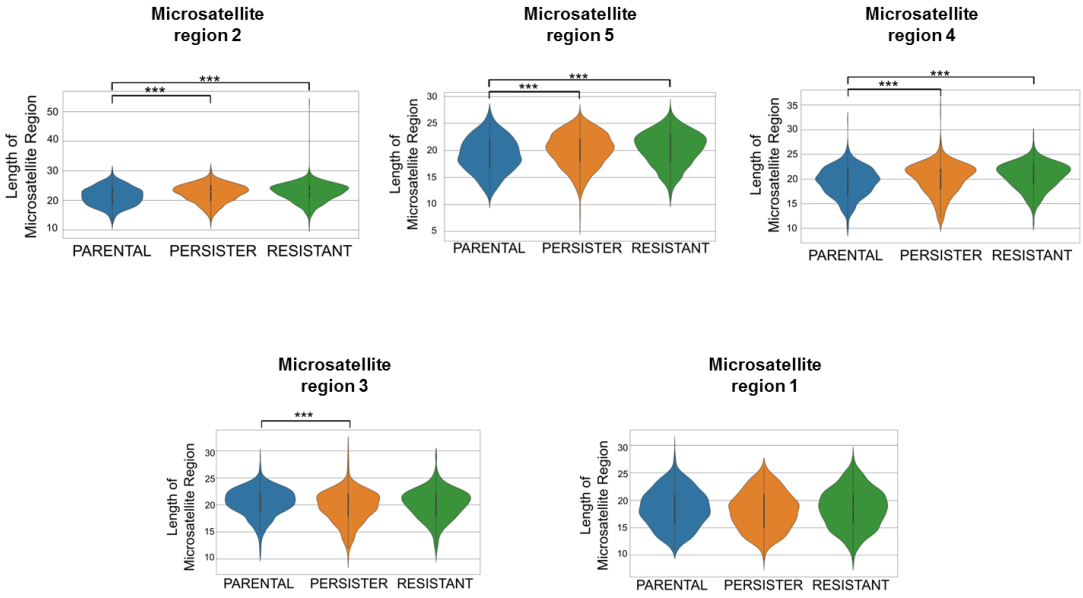

Fig. S17. Alteration of microsatellite regions in WiDr cells. Lengths distribution of the 5 unstable sites included in the NGS high depth capture panel are reported. Chr, Chromosome. *** $p<0.001$ ($\chi 2$ test).

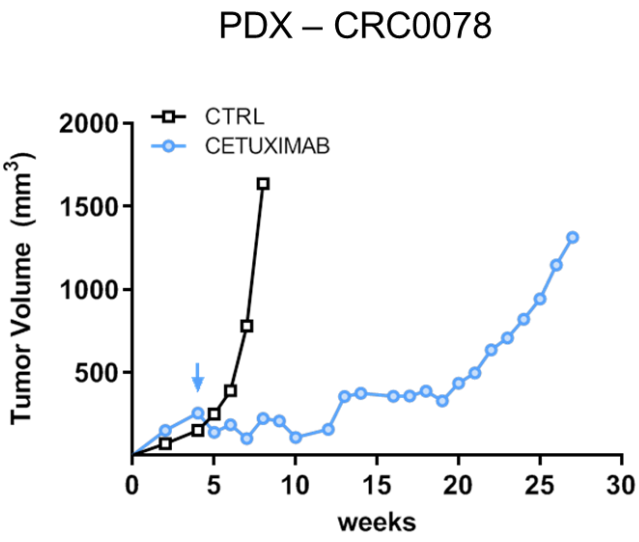

Fig. S18. Emergence of secondary resistance to cetuximab in a patient-derived xenograft. Patient-derived mice models (PDX) were established from a tumor obtained from a metastatic colorectal cancer patient (CRC0078) with a *RAS*/*RAF* wild-type tumor. Upon successful engraftment, mice were randomized to vehicle (CTRL) or cetuximab-treated arm as reported. Results represent tumor mass volume (mm^3) of one PDX that developed cetuximab resistance and of the corresponding vehicle-treated control mouse. Blue arrow indicates treatment start.

Sample ID	Coverage (depth > 40X)	Coverage (depth > 1X)	Median Depth
	Whole Exome Sequencing		
DiFi_parental	92.6301	98.4883	111
DiFi_Persisters	90.4104	98.5003	97
DiFi_Resistant	91.8776	98.3399	113
WiDr_parental	94.5697	98.5403	118
WiDr_Persisters	93.0298	98.5398	104
WiDr_Resistant	95.1203	98.5626	125
PDX Vehicle CTRL	87.62	97.78	114
PDX CTX-R	89.11	98.21	94
	High depth capture panel		
WiDr_parental	99.5962	99.5223	8657
WiDr_Persisters	99.5962	99.5259	11337
WiDr_Resistant	99.5962	99.5259	11802

Table S1. NGS sequencing depth. The table lists exome sequencing median depth for the indicated CRC models. Mouse-derived reads were filtered out in case of patient-derived xenograft (PDX Vehicle CTRL and PDX CTX-R) data.

Chrom.	Start	Stop	Description	Chrom.	Start	Stop	Description
chr14	105258934	105259059	AKT1-exon2	chr17	37872553	37872686	ERBB2
chr14	105246425	105246553	AKT1-exon3	chr17	37872767	37872858	ERBB2
chr14	105242995	105243107	AKT1-exon4	chr17	37873572	37873733	ERBB2
chr3	41265559	41265573	CTNNB1-exon2	chr17	37876039	37876087	ERBB2
chr3	41266016	41266244	CTNNB1-exon3	chr17	37879571	37879710	ERBB2
chr7	55227831	55228031	EGFR-exon12	chr17	37879790	37879913	ERBB2
chr7	55241613	55241736	EGFR-exon18	chr17	37880164	37880263	ERBB2
chr7	55242414	55242513	EGFR-exon19	chr17	37880978	37881164	ERBB2
chr7	55248985	55249171	EGFR-exon20	chr17	37881301	37881457	ERBB2
chr7	55259411	55259567	EGFR-exon21	chr17	37881579	37881655	ERBB2
chr16	30129669	30129859	MAPK3-exon3	chr17	37881959	37882106	ERBB2
chr16	30129367	30129484	MAPK3-exon4	chr17	37882814	37882912	ERBB2
chr16	30128214	30128324	MAPK3-exon7	chr17	37883067	37883256	ERBB2
chr16	30127988	30128111	MAPK3-exon8	chr17	37883547	37883800	ERBB2
chr22	22160139	22160329	MAPK1-exon3	chr17	37883941	37884297	ERBB2
chr22	22127161	22127271	MAPK1-exon7	chr7	116339138	116340338	MET
chr6	152265307	152265643	ESR1-exon6	chr7	116371721	116371913	MET
chr6	152419866	152420101	ESR1-exon10	chr7	116380003	116380138	MET
chr7	14850871	14850881	EZH2-exon16	chr7	11638090	11638107	MET

	6	2			5	9	
chr10	123279492	123279683	FGFR2-exon7	chr7	116395408	116395569	MET
chr10	123274630	123274833	FGFR2-exon9	chr7	116397490	116397593	MET
chr10	123258008	123258119	FGFR2-exon12	chr7	116397691	116397828	MET
chr10	123247504	123247627	FGFR2-exon14	chr7	116398512	116398674	MET
chr4	1803561	1803752	FGFR3-exon7	chr7	116399390	116399544	MET
chr4	1806056	1806247	FGFR3-exon9	chr7	116403103	116403322	MET
chr4	1807777	1807900	FGFR3-exon14	chr7	116409698	116409845	MET
chr4	1808272	1808410	FGFR3-exon16	chr7	116411551	116411708	MET
chr19	3114941	3115070	GNA11-exon4	chr7	116411902	116412043	MET
chr19	3118921	3119051	GNA11-exon5	chr7	116414934	116415165	MET
chr9	80409378	80409508	GNAQ-exon5	chr7	116417442	116417523	MET
chr20	57484404	57484478	GNAS-exon8	chr7	116418829	116419011	MET
chr20	57484575	57484634	GNAS-exon9	chr7	116422041	116422151	MET
chr11	534211	534322	HRAS-exon2	chr7	116423357	116423523	MET
chr11	533765	533944	HRAS-exon3	chr7	116435708	116435845	MET
chr2	209113092	209113384	IDH1-exon4	chr7	116435940	116436178	MET
chr15	90631818	90631979	IDH2-exon4	chr17	7572926	7573008	TP53
chr4	55564449	55564731	KIT-exon3	chr17	7573926	7574033	TP53
chr4	55593581	55593708	KIT-exon8	chr17	7576536	7576584	TP53
chr4	55594176	55594287	KIT-exon11	chr17	7576624	7576657	TP53
chr4	55595500	55595651	KIT-exon13	chr17	7576852	7576926	TP53
chr4	55599235	55599358	KIT-exon14	chr17	7577018	7577155	TP53
chr4	55592024	55592217	KIT-exon15	chr17	7577498	7577608	TP53
chr4	55597494	55597586	KIT-exon17	chr17	7578176	7578289	TP53
chr12	25398207	25398318	KRAS-exon2	chr17	7579699	7579721	TP53
chr12	25380167	25380346	KRAS-exon3	chr17	7579838	7579912	TP53
chr12	25378547	25378707	KRAS-exon4	chr17	7579311	7579590	TP53
chr15	66727364	66727575	MAP2K1-exon2	chr17	7578370	7578556	TP53
chr15	66729083	66729230	MAP2K1-exon3	chr17	7565259	7565332	TP53
chr15	66774093	66774218	MAP2K1-exon6	chr17	7569526	7569562	TP53
chr19	4123780	4123872	MAP2K2-exon1	chr2	47630329	47630541	MSH2
chr19	4117416	4117627	MAP2K2-exon2	chr2	47635538	47635694	MSH2
chr19	4101016	4101141	MAP2K2-exon6	chr2	47637231	47637511	MSH2
chr19	4099198	4099412	MAP2K2-exon7	chr2	47639551	47639699	MSH2
chr2	178098732	178098999	NFE2L2-exon2	chr2	47641406	47641557	MSH2
chr1	115258669	115258781	NRAS-exon2	chr2	47643433	47643568	MSH2
chr1	115256419	115256599	NRAS-exon3	chr2	47656879	47657080	MSH2
chr1	115252188	115252349	NRAS-exon4	chr2	47672685	47672796	MSH2
chr1	156846191	156846364	NTRK1-exon13	chr2	47690168	47690293	MSH2

chr1	156848913	156849154	NTRK1-exon14	chr2	47693795	47693947	MSH2
chr4	55141007	55141140	PDGFRA-exon12	chr2	47698102	47698201	MSH2
chr4	55144062	55144173	PDGFRA-exon14	chr2	47702162	47702409	MSH2
chr4	55152007	55152130	PDGFRA-exon18	chr2	47703504	47703710	MSH2
chr3	178935997	178936122	PIK3CA-exon9	chr2	47705409	47705658	MSH2
chr3	178951881	178952152	PIK3CA-exon20	chr2	47707833	47708010	MSH2
chr12	133253131	133253239	POLE-exon9	chr2	47709916	47710088	MSH2
chr12	133250160	133250293	POLE-exon13	chr2	48010371	48010632	MSH6
chr12	133249749	133249863	POLE-exon14	chr2	48018064	48018262	MSH6
chr12	133219992	133220146	POLE-exon34	chr2	48023031	48023202	MSH6
chr10	89692769	89693008	PTEN-exon5	chr2	48025748	48028294	MSH6
chr10	89711874	89712016	PTEN-exon6	chr2	48030557	48030824	MSH6
chr10	89717609	89717776	PTEN-exon7	chr2	48032047	48032166	MSH6
chr10	89720650	89720875	PTEN-exon8	chr2	48032755	48032846	MSH6
chr12	112888121	112888316	PTPN11-exon3	chr2	48033341	48033497	MSH6
chr12	112926827	112926979	PTPN11-exon13	chr2	48033589	48033790	MSH6
chr10	43595906	43596170	RET-exon2	chr2	48033916	48033999	MSH6
chr10	43609927	43610184	RET-exon11	chr3	37035037	37035154	MLH1
chr10	43617393	43617464	RET-exon15	chr3	37038108	37038200	MLH1
chr10	43615529	43615652	RET-exon16	chr3	37042444	37042544	MLH1
chr17	56448271	56448394	RNF43-exon2	chr3	37045890	37045965	MLH1
chr17	56440886	56440961	RNF43-exon3	chr3	37048480	37048554	MLH1
chr17	56440635	56440767	RNF43-exon4	chr3	37050303	37050396	MLH1
chr17	56439904	56440009	RNF43-exon5	chr3	37053309	37053353	MLH1
chr17	56434828	56436184	RNF43-exon8	chr3	37053500	37053590	MLH1
chr18	48575055	48575230	SMAD4-exon3	chr3	37055921	37056035	MLH1
chr18	48591792	48591976	SMAD4-exon9	chr3	37058995	37059090	MLH1
chr18	48593388	48593557	SMAD4-exon10	chr3	37061799	37061954	MLH1
chr18	48603007	48603146	SMAD4-exon11	chr3	37067126	37067498	MLH1
chr18	48604625	48604837	SMAD4-exon12	chr3	37070273	37070423	MLH1
chr7	128846304	128846428	SMO-exon6	chr3	37081675	37081785	MLH1
chr7	128850203	128850389	SMO-exon9	chr3	37083757	37083822	MLH1
chr7	128851476	128851611	SMO-exon11	chr3	37089008	37089174	MLH1
chr20	36031573	36031782	SRC-exon12	chr3	37090006	37090100	MLH1
chr20	36030838	36030992	SRC-exon14	chr3	37090393	37090508	MLH1
chr19	1206912	1207202	STK11-exon1	chr3	37091975	37092144	MLH1
chr19	1220371	1220504	STK11-exon4	chr7	116411708	116411902	MET_intron13
chr19	1221211	1221339	STK11-exon6	chr7	116412043	116412143	MET_intron14
chr19	1222983	1223171	STK11-exon8	chr5	174778603	174778753	rs251934
chr5	1294952	1295378	TERT-5-utr	chr13	106938336	106938486	rs354439
chr2	47641426	47641608	Microsatellite_region1	chr5	2879320	2879470	rs717302
chr4	55598122	55598274	Microsatellite_regio	chr19	28463262	28463412	rs719366

			n2				
chr2	95849306	95849434	Microsatellite_region3	chr21	16685523	16685673	rs722098
chr14	23652309	23652419	Microsatellite_region4	chr6	165045259	165045409	rs727811
chr11	102193485	102193574	Microsatellite_region5	chr16	5606122	5606272	rs729172
chr5	112043414	112043579	APC	chr22	27816709	27816859	rs733164
chr5	112090587	112090722	APC	chr10	3374103	3374253	rs735155
chr5	112102022	112102107	APC	chr7	155990738	155990888	rs737681
chr5	112102885	112103087	APC	chr10	2406556	2406706	rs826472
chr5	112111325	112111434	APC	chr14	98845456	98845606	rs873196
chr5	112116486	112116600	APC	chr2	114899	115049	rs876724
chr5	112128142	112128226	APC	chr1	239881851	239882001	rs891700
chr5	112136975	112137080	APC	chr11	11096146	11096296	rs901398
chr5	112151191	112151290	APC	chr2	239563504	239563654	rs907100
chr5	112154662	112155041	APC	chr21	42415854	42416004	rs914165
chr5	112157592	112157688	APC	chr7	4456928	4457078	rs917118
chr5	112162804	112162944	APC	chr10	132698344	132698494	rs964681
chr5	112163625	112163703	APC	chr20	39487035	39487185	rs1005533
chr5	112164552	112164669	APC	chr18	75432311	75432461	rs1024116
chr5	112170647	112170862	APC	chr22	48362215	48362365	rs1028528
chr5	112173249	112179823	APC	chr6	1135864	1136014	rs1029047
chr7	140434396	140434570	BRAF	chr20	4447408	4447558	rs1031825
chr7	140439611	140439746	BRAF	chr13	20901649	20901799	rs1335873
chr7	140449086	140449218	BRAF	chr3	190806033	190806183	rs1355366
chr7	140453074	140453193	BRAF	chr3	961707	961857	rs1357617
chr7	140453986	140454033	BRAF	chr9	128967988	128968138	rs1360288
chr7	140476711	140476888	BRAF	chr16	80106286	80106436	rs1382387
chr7	140477790	140477875	BRAF	chr1	242806722	242806872	rs1413212
chr7	140481375	140481493	BRAF	chr14	25850757	25850907	rs1454361
chr7	140482820	140482957	BRAF	chr9	126881373	126881523	rs1463729
chr7	140487347	140487384	BRAF	chr1	4367248	4367398	rs1490413
chr7	140494107	140494267	BRAF	chr18	1127911	1128061	rs1493232
chr7	140500161	140500281	BRAF	chr15	55210630	55210780	rs1528460
chr7	140501211	140501360	BRAF	chr13	22374625	22374775	rs1886510

chr7	140507759	140507862	BRAF	chr4	190318005	190318155	rs1979255
chr7	140508691	140508795	BRAF	chr15	24571721	24571871	rs2016276
chr7	140534408	140534672	BRAF	chr22	47836337	47836487	rs2040411
chr7	140549910	140550012	BRAF	chr8	139399041	139399191	rs2056277
chr7	140624365	140624503	BRAF	chr11	134667471	134667621	rs2076848
chr17	37855812	37855840	ERBB2	chr12	888245	888395	rs2107612
chr17	37856491	37856564	ERBB2	chr12	106328179	106328329	rs2111980
chr17	37863242	37863394	ERBB2	chr21	28608088	28608238	rs2830795
chr17	37864573	37864787	ERBB2	chr15	53616834	53616984	rs8037429
chr17	37865570	37865705	ERBB2	chr1	238439233	238439383	rs10495407
chr17	37866065	37866134	ERBB2	chrX	1537806	1537956	rs4503285
chr17	37866338	37866454	ERBB2	chrX	152584785	152584935	rs114536331
chr17	37866592	37866734	ERBB2	chr17	80461859	80462010	rs8078417
chr17	37868180	37868300	ERBB2	chr17	440422	440572	rs7219151
chr17	37868574	37868701	ERBB2	chr21	43481545	43481695	rs69686
chr17	37871538	37871612	ERBB2	chr4	46329580	46329730	rs279844
chr17	37871698	37871789	ERBB2	chr8	17182466	17182616	rs2239865
chr17	37871992	37872192	ERBB2	chr9	991039	991189	rs279877

Table S2. NGS custom high depth capture panel. The table lists the regions captured by the panel.